Bioorganic & Medicinal Chemistry 18 (2010) 2686–2703

Contents lists available at ScienceDirect

Bioorganic & Medicinal Chemistry

journal homepage: www.elsevier.com/locate/bmc

Statistical molecular design of a focused salicylidene acylhydrazide library and multivariate QSAR of inhibition of type III secretion in the Gram-negative bacterium *Yersinia*

Markus K. Dahlgren, Caroline E. Zetterström, Åsa Gylfe, Anna Linusson, Mikael Elofsson *

Department of Chemistry, Umeå University, SE-901 87 Umeå, Sweden

ARTICLE INFO

Article history:
Received 4 November 2009
Revised 10 February 2010
Accepted 12 February 2010
Available online 18 February 2010

Keywords:
Statistical molecular design
QSAR
Type III secretion
Bacterial virulence
Antibacterial
Yersinia
Chlamydia

ABSTRACT

A combined application of statistical molecular design (SMD), quantitative structure–activity relationship (QSAR) modeling and prediction of new active compounds was effectively used to develop salicylidene acylhydrazides as inhibitors of type III secretion (T3S) in the Gram-negative pathogen *Yersinia pseudotuberculosis*. SMD and subsequent synthesis furnished 50 salicylidene acylhydrazides in high purity. Based on data from biological evaluation in T3S linked assays 18 compounds were classified as active and 25 compounds showed a dose-dependent inhibition. The 25 compounds were used to compute two multivariate QSAR models and two multivariate discriminant analysis models were computed from both active and inactive compounds. Three of the models were used to predict 4416 virtual compounds in consensus and eight new compounds were selected as an external test set. Synthesis and biological evaluation of the test set in *Y. pseudotuberculosis* and the intracellular pathogen *Chlamydia trachomatis* validated the models. *Y. pseudotuberculosis* and *C. trachomatis* cell-based infection models showed that compounds identified in this study are selective and non-toxic inhibitors of T3S dependent virulence.

1. Introduction

Antibiotic resistance has evolved against the majority of all clinically used antibiotics and it is clear that mankind is loosing ground in the never-ending battle against bacterial infections. Current antibiotics all target bacterial growth with low selectivity and thereby affect both pathogenic bacteria and our benign endogenous microflora. Alternative strategies are needed and recent findings suggest that bacterial mechanisms required for infection, virulence factors, can effectively be targeted.[1–3]

Type III secretion (T3S) is a virulence system found in a wide range of clinically important Gram-negative pathogens including *Yersinia* spp., *Chlamydia* spp., *Shigella* spp., *Salmonella* spp., *Pseudomonas aeruginosa*, and enteropathogenic and enterohemorrhagic *Escherichia coli*.[4] The T3S machinery is a syringe-like organelle that delivers toxins into the host cell cytosol and the bacteria thereby modulate the host responses and create a specific niche for colonization. In contrast to the toxins, which in most cases are unique for each bacterial species, the T3S machinery is evolutionary conserved and therefore constitutes a potential drug target.[1–3,5] Screening-based approaches using phenotype cell-based assays have resulted in synthetic and natural compounds that target T3S in *Yersinia* spp., enteropathogenic *E. coli*, *Salmonella typhimurium*, *P. aeruginosa*, and *P. syringae*.[6–11] Continued efforts have led to optimized compounds, tethered inhibitors, synthetic methods, and structure–activity relationships.[12–19] Recently it was reported that plant phenolic acids induce expression of T3S system genes in the plant pathogen *Dickeya dadantii* by moderation of a two-component system[20] and based on this finding *p*-coumaric acid was identified as a repressor of T3S system genes.[21] Another recent publication describes that the proton pump inhibitor omeprazole blocks T3S in *S. enterica*.[22] The salicylidene acylhydrazides (Fig. 1), are promising since they target T3S in *Yersinia pseudotuberculosis*,

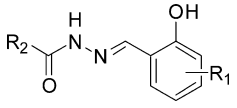

Figure 1. The general structure of salicylidene acylhydrazides.

Abbreviations: BB, building block; T3S, type III secretion; T2S, type II secretion; T4S, type IV secretion; PLS, partial least-square regression to latent ce:text>; Hi-PLS, hierarchical PLS; PLS-DA, PLS discriminant analysis; ETEC, enterotoxigenic *Escherichia coli*; YPIII, *Yersinia pseudotuberculosis* serotype III; BHI, brain heart infusion; DOOD, D-optimal onion design; PCA, principal component analysis; SAR, structure–activity relationship; QSAR, quantitative structure–activity relationship; SMD, statistical molecular design; MLR, multiple linear regression; SVM, support vector machine; MM, molecular mechanics; Yop, *Yersinia* outer protein; FCS, fetal calf serum; DMEM, Dulbecco's modified Eagle's medium; LB, Luria broth; OD, optical density; RPMI, Roswell Park Memorial Institute; MIC, minimum inhibitory concentration.

* Corresponding author. Tel.: +46 90 7869328; fax: +46 90 7867655.
E-mail address: mikael.elofsson@chem.umu.se (M. Elofsson).

0968-0896/$ - see front matter © 2010 Elsevier Ltd. All rights reserved.
doi:10.1016/j.bmc.2010.02.022

Shigella flexneri, enterohemorrhagic *E. coli*, and *Salmonella* spp. that inflict a broad range of gastrointestinal infections and *Chlamydia* spp. that cause sexually transmitted disease.[13,23–27] In addition, to the potential of these T3S inhibitors to be developed into therapeutic agents they are important chemical probes to further study the role of T3S in different systems. This is particularly important for organisms like the obligate intracellular pathogen *Chlamydia* spp. for which no tractable genetic system exists.[23,28–32]

The biological target of the salicylidene acylhydrazides is currently unknown and the biological evaluations have been performed on whole bacterial cells. It cannot be excluded that the compounds act on multiple targets or that the target(s) might vary between different species. To further develop this compound class it is necessary to gain a detailed understanding of what chemical features that affect biological activity and how these can be merged with, for example, pharmacokinetic requirements for in vivo experiments. One strategy to achieve this is the computation of quantitative structure–activity relationship (QSAR)[33–35] models based on compound sets obtained by statistical molecular design (SMD)[36,37] and biological data, typically from assays in vitro. Despite its obvious advantages the combined application of SMD and QSAR modeling have been described in relatively few publications.[16,17,37–41]

The strength of SMD is that it results in a statistically balanced compound set suitable for QSAR modeling and importantly SMD can be performed without knowledge of the target. One way to perform SMD is to mathematically describe building blocks (BBs), that is, the reactants used to construct the compound class of interest, with calculated or experimentally derived molecular descriptors and then make a selection based on chemical properties. The procedure is repeated for each BB set and an enumeration of the selected BBs results in a virtual library. The products are then characterized with descriptors and a new diverse selection is performed in order to lower the number of synthetic targets and still retain most of the information of the full data set. Alternatively products can be selected by a statistically controlled combination of the selected BBs without requirement for characterization of the virtual products. Another advantage of making the selection in the BB space rather than the product space is that the interpretation of the QSAR will give information about the desired properties of BBs.

QSAR models are constructed from a set of biologically active molecules, the training set, identified among compounds obtained by, for example, SMD. The molecules are mathematically described by calculated or experimentally derived molecular descriptors and a regression technique, for example, multiple linear regression (MLR),[42] partial least-squares regression to latent structures (PLS),[43,44] or support vector machine (SVM),[45] is used to correlate the training set and its variables to the biological response. QSAR models are generally only valid in the experimental domain covered by the molecules in the training set since such models are interpolating. This means that the training set has to cover the molecular properties important for the biological response, that is, the training set should represent a variety of chemical properties that might influence the biological response in order to get a spread in biological activity. At the same time the training set should not contain too diverse compounds as it potentially could lead to many inactive compounds and this can be prevented by applying basic SARs prior to SMD.

It is common that several QSAR models are computed, for example, when applying different regression methods, adding or removing training set molecules, transforming molecular descriptors or the biological response mathematically, and adding or removing descriptors. Often it can be difficult to decide which model to use for predictions, as statistics of the models may be similar while the predictions of new compounds may differ. The different models could possibly all be useful, depending on the task, as the models could potentially excel at predicting parts of the prediction set. Recent publications highlight the usefulness of consensus predictions using several QSAR models.[46–48] The more orthogonal models are relative to each other, the higher the predictive power should be when they are used in consensus.[48]

In this paper, we use SMD to select diverse sets of salicylic aldehydes and hydrazides for synthesis of salicylidene acylhydrazides. Of the 54 selected compounds 50 compounds could successfully be synthesized and purified. All compounds were evaluated for T3S inhibition in *Y. pseudotuberculosis* and several multivariate QSAR models were computed. The predictive ability of the models was evaluated and confirmed in consensus using an external set of compounds. A panel of compounds was evaluated for virulence inhibition in cell infection models.

2. Results and discussion

2.1. Statistical molecular design

The salicylidene acylhydrazides were assembled in one step from salicylic aldehydes and hydrazides. Based on published data it was clear that the aromatic rings of both the BBs tolerated substitution with different functional groups or exchange to heteroaromatic systems or fused aromatics without loss of biological activity.[13,24,29] After careful inspection of the compounds and their corresponding biological activity, we could not deduce any clear SAR in terms of substituent patterns. The salicylic aldehyde moiety tolerated both polar and hydrophobic substituents while retaining biological activity. This indicated that properties like pK_a of the salicylic phenol and partial charges of the carbon atoms in the salicylic aldehyde aromatic ring might be of larger importance than the hydrophobicity of the functional groups. There seemed to be a highly non-linear relationship between the BBs constituting the molecules and their biological response. Current data thus suggested complex SARs and in view of that the target was unknown it was of importance to select a statistically balanced set of compounds, covering a wide range of properties, in order to get a compound library with a spread in biological activity well suited for QSAR modeling. From commercial vendors 48 salicylic aldehydes (Fig. S1) and 92 hydrazides (Fig. S2) were selected (Section 4.1), numerically described using calculated molecular descriptors and subjected to SMD as schematically shown in Figure 2.

Low energy conformations of the 48 salicylic aldehydes were numerically described with computed ab initio, molecular mechanics (MM) and informatics descriptors resulting in total 70 descriptors (Table S1). In order to ensure that the MM descriptors were not overrepresented and to reduce the impact of the hydrophobicity descriptors, a selection of MM descriptors were grouped in two separate groups and summarized using PCA (Fig. 2a, Tables S2–S4). The total data was compressed block wise using PCA, resulting in a five component model ($R^2 = 0.85$, $Q^2 = 0.53$) for the salicylic aldehyde BBs (Fig. 2a and Table S5). Conformational analysis of the 92 hydrazides was followed by a numerical description of the structures through computation of a total of 97 ab initio, MM, and informatics descriptors (Table S6). After removal of a number of non-interpretable descriptors the remaining subset consisting of 50 descriptors (Table S7) were summarized in one block using PCA (Fig. 2b), resulting in a five component model ($R^2 = 0.88$, $Q^2 = 0.77$). The PCA score vectors were used as design variables, and for each data set a two-layer D-optimal onion design (DOOD)[49] was performed. Seventeen salicylic aldehydes and 18 hydrazides were selected by the designs. One salicylic aldehyde, 5-bromo-salicylic aldehyde, which has been found in several salicylidene acylhydrazides that inhibited T3S[13,24] was added manually to make

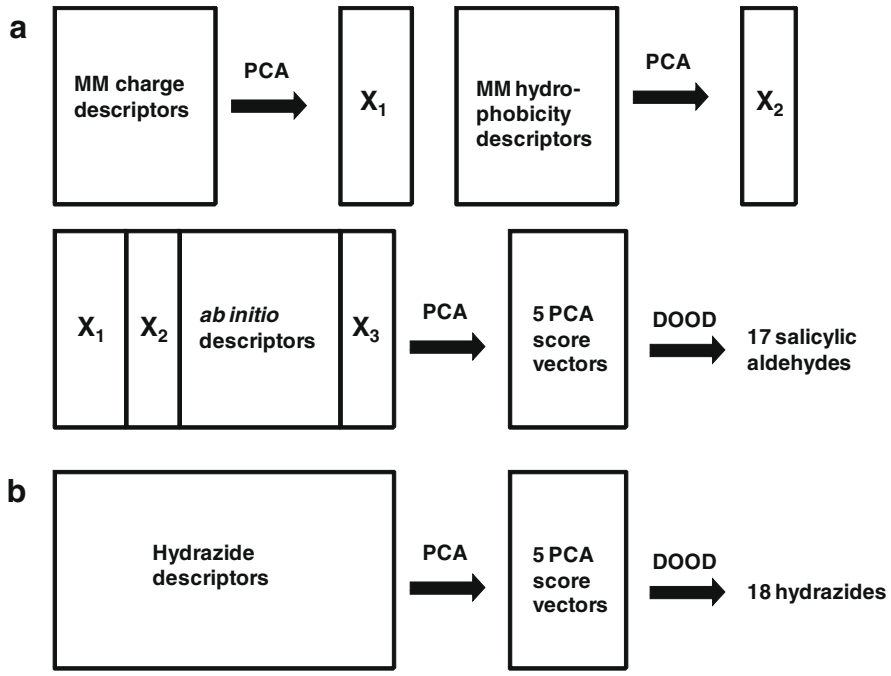

Figure 2. Schematic representation of the design process for (a) salicylic aldehydes and (b) hydrazides. For the salicylic aldehydes the MM descriptors describing charges and hydrophobicity were grouped and summarized with PCA separately. The resulting score vectors (blocks X_1 and X_2) were combined with the ab initio descriptors and X_3 (molecular weight and volume). PCA was used to summarize the variation of both BB sets and two libraries of BBs were designed using two separate two-layer DOODs.

the two BB sets of equal size. A final selection resulted in 54 virtual products (Section 4.2).

2.2. Synthesis

The salicylidene acylhydrazides were synthesized in one step from salicylic aldehydes and hydrazides by conventional or microwave heating in absolute ethanol. The purified compounds were analyzed and characterized with LC–MS and ^{1}H NMR spectroscopy using DMSO as solvent. A dynamic process gave rise to two rotamers for 34 of the salicylidene acylhydrazides. A total of 50 compounds were successfully synthesized in 60–95% yield with a purity of at least 95% (Tables 1 and S8). The three compounds containing the BB butyric acid hydrazide could not be synthesized as the BB proved to be unreactive under the reaction conditions used (Fig. S3). 4-Methyl-[1,2,3]thiadiazole-5-carboxylic acid (2-hydroxy-3-methoxy-5-nitro-benzylidene)-hydrazide (Fig. S3) could not be purified above 80% according to the integrated UV-trace from LC and this compound was therefore omitted from further studies.

2.3. Biological evaluation for QSAR modeling

The 50 salicylidene acylhydrazides were evaluated at eight concentrations (1.56–200 μM) in *Y. pseudotuberculosis* using a T3S linked luciferase reporter-gene assay[6,13] (Tables 1 and S9a, and Fig. S24) and an enzymatic assay based on the secreted phosphatase, YopH.[16] Compounds were classified as active if they showed a dose-dependent effect with more than 40% inhibition at 50 μM in the luciferase reporter-gene assay and a concomitant dose-dependent reduction of the YopH activity (Fig. S4a). Based on these criteria 18 of the 50 compounds were classified as active. Five compounds (**ME0163** and **ME0190**–**ME0193**) did not show an inhibitory effect in the YopH assay (Fig. S4b) and possibly inhibit the luciferase directly in a T3S independent mechanism. For **ME0151** (Fig. S24) the inhibitory effect diminished in both the reporter-gene and YopH assay at concentrations above 100 μM and this is most likely due to limited aqueous solubility. In addition, all compounds were tested for growth inhibition of *Y. pseudotuberculosis* and *E. coli* at 50 and 100 μM and no or modest effects were observed (Fig. S5).

2.4. Multivariate QSAR for T3S inhibition

All our modeling efforts showed that there was a non-linear relationship between the molecular descriptions of the BBs constituting the inhibitors and their biological response. Initially two models for predictions, **Hi-PLS-1** and **Hi-PLS-DA-1**, were computed based on PLS score vectors by application of our previously published methodology[17] as schematically described in Figure 3 (model statistics in Table 2). **Hi-PLS-1** showed good correlation between experimental and calculated luciferase signal inhibition (Fig. 4) and **Hi-PLS-DA-1** showed good separation of active compounds and inactive compounds along the direction of the PLS score vector (Fig. 5). To get interpretable models, grouped descriptors were used to compute two new models, **Hi-PLS-2** and **Hi-PLS-DA-2**, as schematically shown in Figure 6. The correlation between calculated and experimental inhibition is good for **Hi-PLS-2** (Fig. 7) while **Hi-PLS-DA-2** was less efficient than **Hi-PLS-DA-1** in separating actives from non-actives (Fig. S6). All models except **Hi-PLS-DA-2** had acceptable and comparable statistics (R^2Y above 0.65 and Q^2 above 0.50, Table 2). Permutations of the response and subsequent model computations were performed and the result showed that the **Hi-PLS-1** and **Hi-PLS-2** models were not a result of chance correlation (Figs. S7 and S8). The loading plots for **Hi-PLS-1** (Fig. S9), and **Hi-PLS-DA-1** (Fig. S10), and **Hi-PLS-DA-2** (Fig. S11) are given in Supplementary data.

The interpretation was based on the model coefficients of **Hi-PLS-2** as shown in Figure 8. The model is dominated by non-linear terms, underlining the complex SAR of the compound class. The calculated pK_a of the phenol in position two of the salicylic aldehydes is the most important property in the model, participating in seven interaction terms. Other important properties are the electrostatic potential charges of the aromatic carbons in the salicylic aldehyde ring that are involved in six interaction terms and

Table 1
Percentage inhibition of luciferase light emission for strain YPIII-pIB102 (*yopE-luxAB*) in the presence of compounds **ME0150**–**ME0199** at 50 μM concentration

ID	Structure	Inhibition[a]	ID	Structure	Inhibition[a]	ID	Structure	Inhibition[a]
ME0150	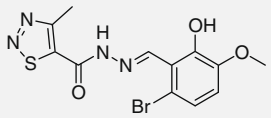	60 ± 1	**ME0164**	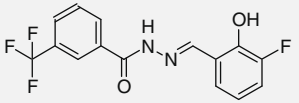	32 ± 1	**ME0178**	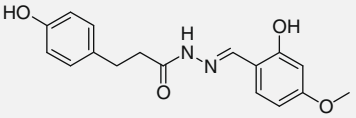	22 ± 6
ME0151	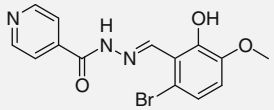	54 ± 2	**ME0165**	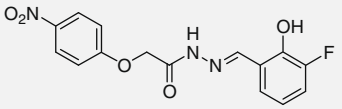	84 ± 0	**ME0179**	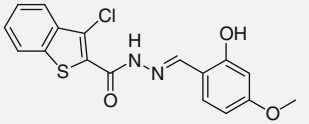	27 ± 3
ME0152	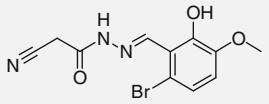	25 ± 3	**ME0166**	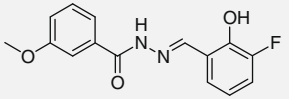	45 ± 2	**ME0180**	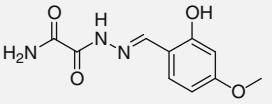	73 ± 1
ME0153	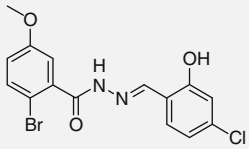	36 ± 3	**ME0167**	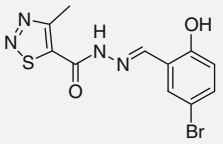	23 ± 9	**ME0181**	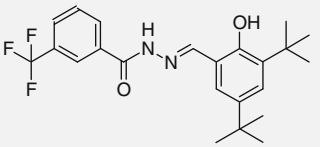	9 ± 3
ME0154	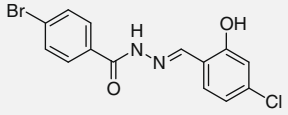	27 ± 6	**ME0168**	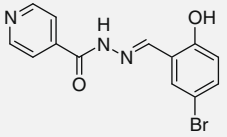	87 ± 0	**ME0182**	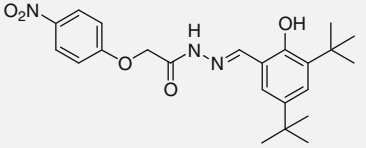	18 ± 8
ME0155	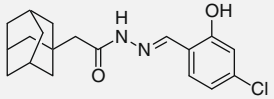	32 ± 2	**ME0169**	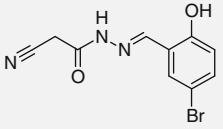	86 ± 1	**ME0183**	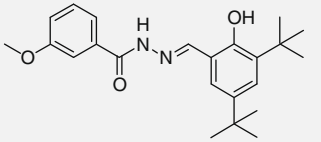	23 ± 4
ME0156	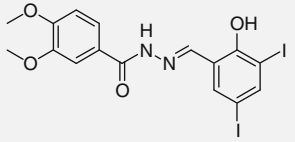	24 ± 10	**ME0170**	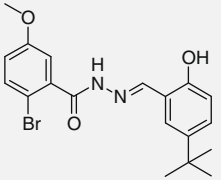	33 ± 3	**ME0184**	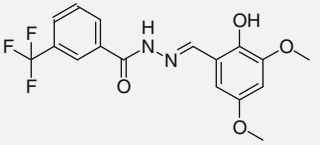	66 ± 1
ME0157	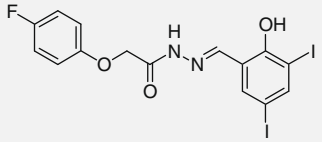	30 ± 5	**ME0171**	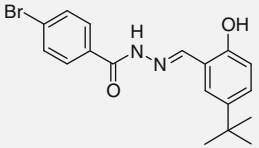	39 ± 3	**ME0185**	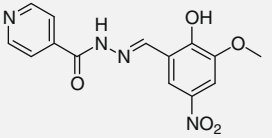	35 ± 7
ME0158	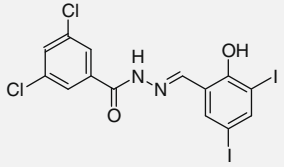	26 ± 8	**ME0172**	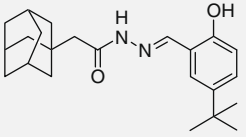	10 ± 3	**ME0186**	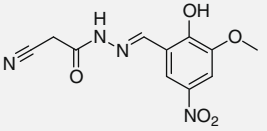	39 ± 2

(*continued on next page*)

Table 1 (*continued*)

ID	Structure	Inhibition[a]	ID	Structure	Inhibition[a]	ID	Structure	Inhibition[a]
ME0159	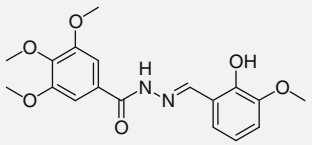	43 ± 3	**ME0173**	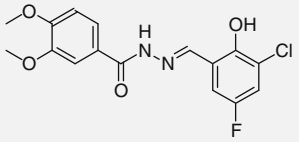	38 ± 11	**ME0187**	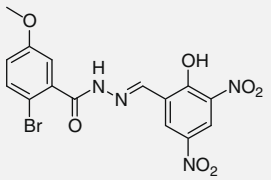	30 ± 1
ME0160	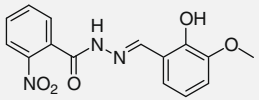	32 ± 4	**ME0174**	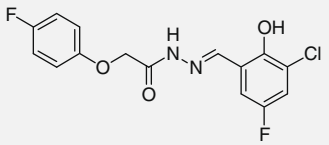	63 ± 4	**ME0188**	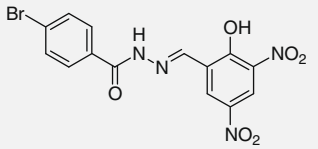	22 ± 1
ME0161	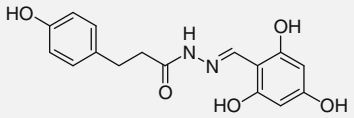	29 ± 1	**ME0175**	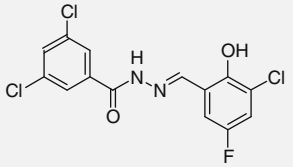	19 ± 3	**ME0189**	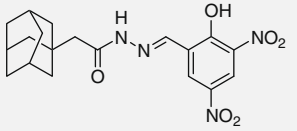	18 ± 4
ME0162	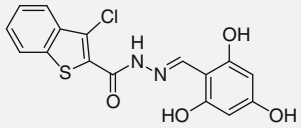	70 ± 2	**ME0176**	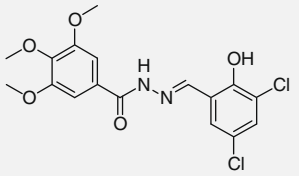	27 ± 0	**ME0190**	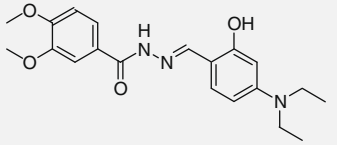	66 ± 1
ME0163	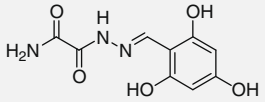	51 ± 2	**ME0177**	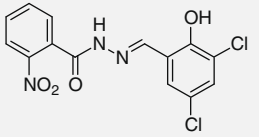	61 ± 2	**ME0191**	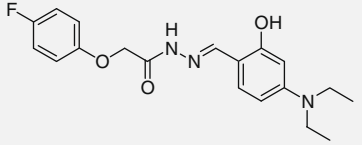	54 ± 2
ME0192	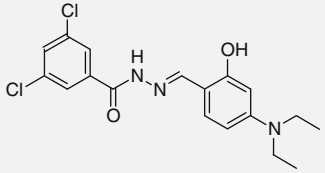	43 ± 1	**ME0195**	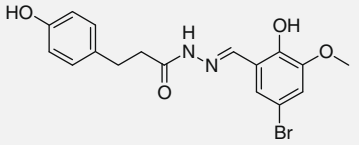	23 ± 2	**ME0198**	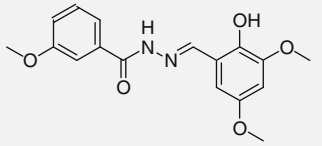	43 ± 2
ME0193	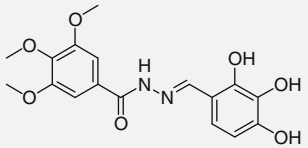	50 ± 3	**ME0196**	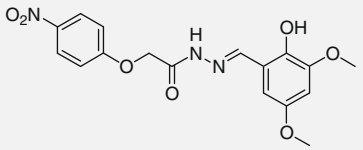	16 ± 3	**ME0199**	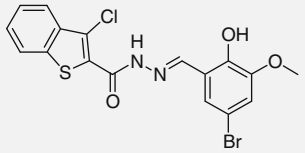	34 ± 2
ME0194	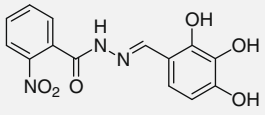	36 ± 1	**ME0197**	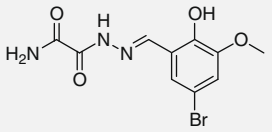	9 ± 8			

[a] Means and standard deviations are calculated from triplicates, and experiments were reproduced on at least three separate occasions.

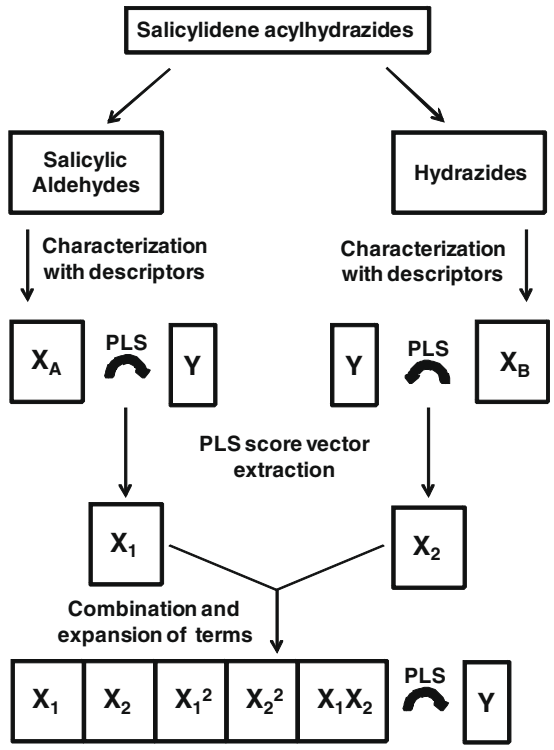

Figure 3. Schematic representation of calculation of **Hi-PLS-1** and **Hi-PLS-DA-1**, using hierarchical PLS score vectors. X_A and X_B are the BB data matrices with calculated descriptors. X_1 and X_2 are the extracted PLS score vectors. Y is the response (i.e., % light emission inhibition at 50 μM for **Hi-PLS-1** and class membership for **Hi-PLS-DA-1**).

Table 2
Statistics for the multivariate models **Hi-PLS-1** and **2** and **Hi-PLS-DA-1** and **2**

Model	Score vector set[a]	R^2X	R^2Y	Q^2
Hi-PLS-1	SAL2 + HYD2	0.19	0.67	0.51
Hi-PLS-DA-1	SAL1 + HYD1	0.12	0.67	0.55
Hi-PLS-2	—	0.29	0.69	0.53
Hi-PLS-DA-2	—	0.21	0.43	0.35

[a] The two combined score vector sets used for the model in question. The score vectors were derived from PLS models (see Section 4.4).

the shape of the salicylic aldehyde moiety which is participating in five interaction terms. The substitution pattern on the salicylic aldehyde ring is therefore of vital importance when designing new salicylidene acylhydrazides as the functional groups on the aromatic ring will affect the electrostatic potential charges, the pK_a of the phenol and the shape of the BB. As a consequence of the non-linear SAR, the salicylic aldehyde BB should not be varied independently of the hydrazide BB, since the biological response is largely dependent on the interactions between the two BBs.

2.5. Evaluation of models using an external test set

Combination of the 48 salicylic aldehydes and 92 hydrazides gave 4416 virtual compounds of which 1916 were predicted as active in **Hi-PLS-1**, 2208 in **Hi-PLS-2**, and 659 in **Hi-PLS-DA-1**. The overlap of the three models was calculated to 327 compounds, indicating a substantial difference between the predictions of the models. From the 327 compounds predicted as active, five (**ME0257**, **ME0259**–**ME0261**, and **ME0264**) were manually selected. Additionally, three compounds predicted as inactive in all models (**ME0258**, **ME0262**, and **ME0263**) were selected and the

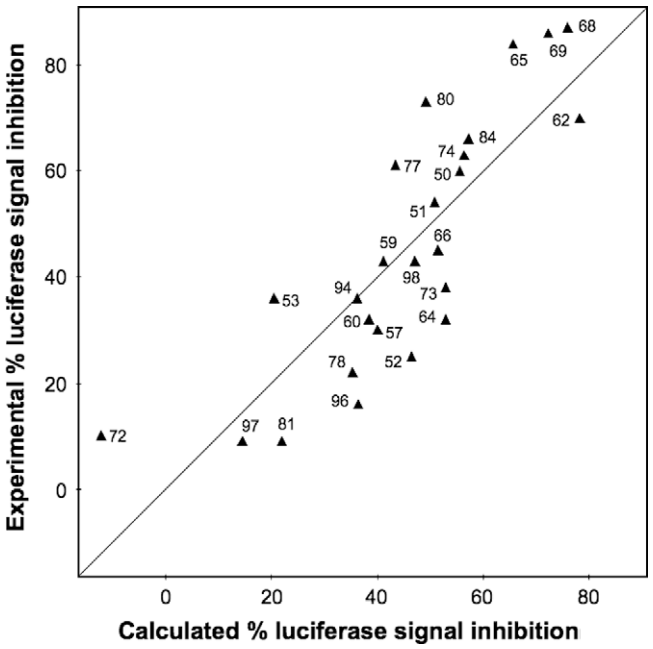

Figure 4. Experimental versus calculated luciferase signal inhibition plot for **Hi-PLS-1** (50 μM compound concentration). The ID numbers in the plot are the last two numbers of the compound IDs.

eight compounds were synthesized and biologically evaluated as described in Sections 4.3 and 4.10 (Tables 3 and S9b). Five of the selected compounds (**ME0258**, **ME0259**, and **ME0261**–**ME0263**) had hydrazide BBs not used in any of the previously 50 synthesized salicylidene acylhydrazides, while all of the salicylic aldehydes were represented in the training set.

The compounds predicted as inactive were all inactive, and of the five compounds predicted as active, three were active (Table 3). In **Hi-PLS-1**, the three 5-bromo-salicylaldehyde containing compounds (**ME0259**–**ME0261**) were predicted as having the highest activity of the eight compounds. According to **Hi-PLS-2** compound **ME0264** should be the most active. Both models predicted **ME0257** to have the lowest activity of the five active compounds. **ME0257** was correctly classified as active, but contrary to predictions it had the highest activity of the five compounds predicted as active and it was one of the four most potent compounds at 50 μM in the total set of 58 salicylidene acylhydrazides. **ME0260** was correctly classified as active and **ME0259**, which was predicted as active, was border line to being active, with a dose-dependent inhibition. **ME0261** and **ME0264** were both incorrectly predicted as active and the lack of activity could possibly be due to factors such as efflux or the compounds having properties not covered by the models. The models correctly classified inactive compounds but could not correctly rank the active compounds. Importantly, the models could handle predictions of compounds having BBs not represented in the training set.

2.6. Inhibition of *Y. pseudotuberculosis* infection

The T3S linked luciferase reporter-gene assay and the enzymatic YopH assay, in combination with assays for general growth inhibition clearly identifies putative virulence inhibitors but these assays are however uncoupled from infection. Four active compounds, **ME0165**, **ME0166**, **ME0168** and **ME0174** and one inactive, **ME0181**, were therefore tested for virulence inhibition in an assay where the mouse macrophage-like cell line J774 is infected with *Y. pseudotuberculosis* (pIB102).[29] A fully functional T3S system translocates the effector proteins into the macrophage cytosol resulting

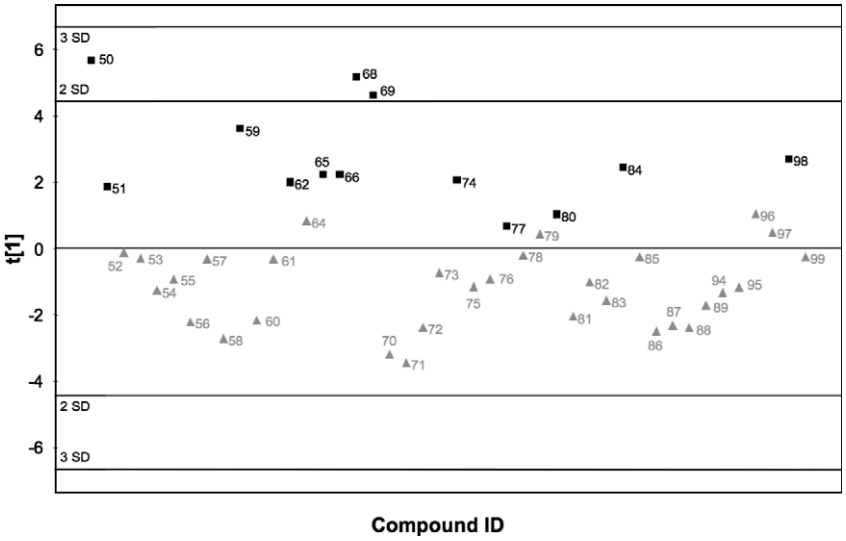

Figure 5. PLS-DA Score plot (**Hi-PLS-DA-1**) of active (black boxes) and inactive (gray triangles) compounds. The plot shows a good separation of active and inactive compounds along the direction of the score vector. The ID numbers in the plot are the last two numbers of the compound IDs.

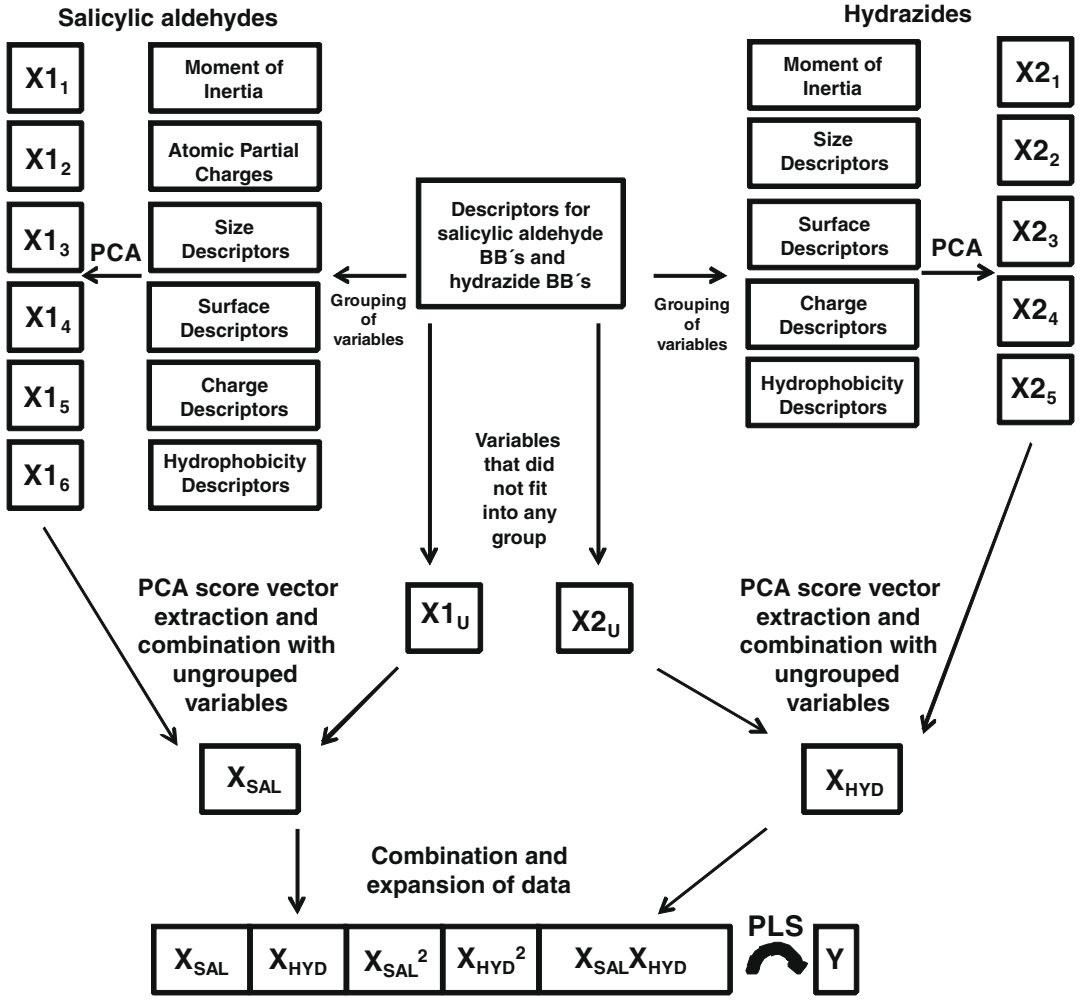

Figure 6. Schematic representation of calculation of **Hi-PLS-2** and **Hi-PLS-DA-2**, using PCA score vectors from grouped variables. Descriptors describing similar properties within the same BB set were grouped and data was summarized using PCA. The PCA score vectors from both BB sets were combined and expanded prior to PLS regression. Y is the response (i.e., % light emission inhibition at 50 μM for **Hi-PLS-2** and class membership for **Hi-PLS-DA-2**).

in cell death or reduced viability. The status of the J774 cells is monitored using CalceinAM, that is, converted to a green fluorescent molecule in healthy cells. Wild-type *Y. pseudotuberculosis* reduced J774 viability and this effect was reversed by **ME0168** that

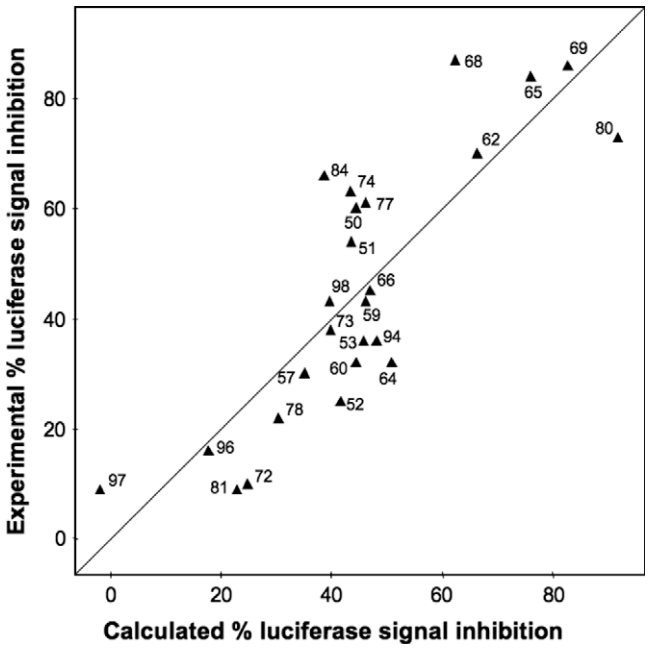

Figure 7. Experimental versus calculated luciferase signal inhibition plot for **Hi-PLS-2** (50 μM compound concentration). The ID numbers in the plot are the last two numbers of the compound IDs.

completely blocked the toxic effects at 50 μM (Fig. 9). Uninfected control cells remained healthy at all compound concentrations indicating that **ME0168** is non-toxic (Fig. 9). Infection by the *Y. pseudotuberculosis* pIB604 Δ*yopB* T3S translocation mutant showed that this strain is non-virulent and **ME0168** had no effect under these conditions (Fig. 9). To further conclude selectivity for T3S dependent virulence mechanisms J774 cells were also infected with enterotoxigenic *E. coli* (ETEC).[50,51] Both *Y. pseudotuberculosis* and ETEC are Gram-negative gastrointestinal pathogens but ETEC lacks a T3S system and instead employs a type II secretion (T2S) system for secretion of toxins.[50] ETEC efficiently reduced macrophage health and this effect was not reversed by addition of **ME0168** indicating that the inhibitor is selective for T3S and do not target toxin secretion in general (Fig. 9). The active compounds **ME0165** and **ME0166** resulted in the same effects as **ME0168** (Fig. S12). The fourth active compound **ME0174** however failed to inhibit virulence which was also true for the inactive compound **ME0181** (Fig. S12). Taken together these results show that our new compounds not only were active when tested on bacteria alone but also selective, non-toxic, and active in a complex cell-based infection model.

2.7. Inhibition of *Chlamydia trachomatis* infection

In order to investigate the specificity for T3S of the salicylidene acylhydrazides, the external test set (**ME0257**–**ME0264**) was evaluated for the ability to inhibit growth of *Chlamydia trachomatis*. In contrast to the extracellular pathogen *Y. pseudotuberculosis*, *C. trachomatis* is an obligate intracellular pathogen that relies on T3S for its growth. *Chlamydia* is therefore a suitable model organism to evaluate if T3S inhibitors identified with *Yersinia* inhibit the evolutionary conserved T3S system in other pathogens. Salicylidene acylhydrazides do not inhibit entry of *Chlamydia* into host cells[31] and the T3S inhibition observed in *Chlamydia* models therefore requires that the compounds penetrate the host cell membrane and enter the compartment, inclusion, hosting the bacteria.[23,28–30] The compounds were added at five different concentrations to HeLa 229 cells one hour post infection with *C. trachomatis*. For each compound the lowest concentration resulting in complete inhibition of *C. trachomatis*, that is, the minimum inhibitory concentration MIC (Table 3). Five of the eight tested salicylidene acylhydrazides (**ME0259**–**ME0261** and **ME0263**–**ME0264**) were able to completely inhibit growth at 50 μM or lower compound concentration. Comparing these results with the biological data from the *Y. pseudotuberculosis* assay, the overlap was determined to two active (**ME0259** and **ME0260**) and two inactive (**ME0258** and **ME0262**) compounds, which was in full agreement with the consensus predictions of the three multivariate models. The models could not correctly predict the biological response of **ME0261** and **ME0264** in *Yersinia*. Interestingly the predictions for **ME0261** and **ME0264** are in accordance with the inhibition of *Chlamydia* growth. The models cannot correctly predict the observed inability of **ME0257** to inhibit *Chlamydia* growth or the activity of **ME0263**. These results show that the models hold information relevant for

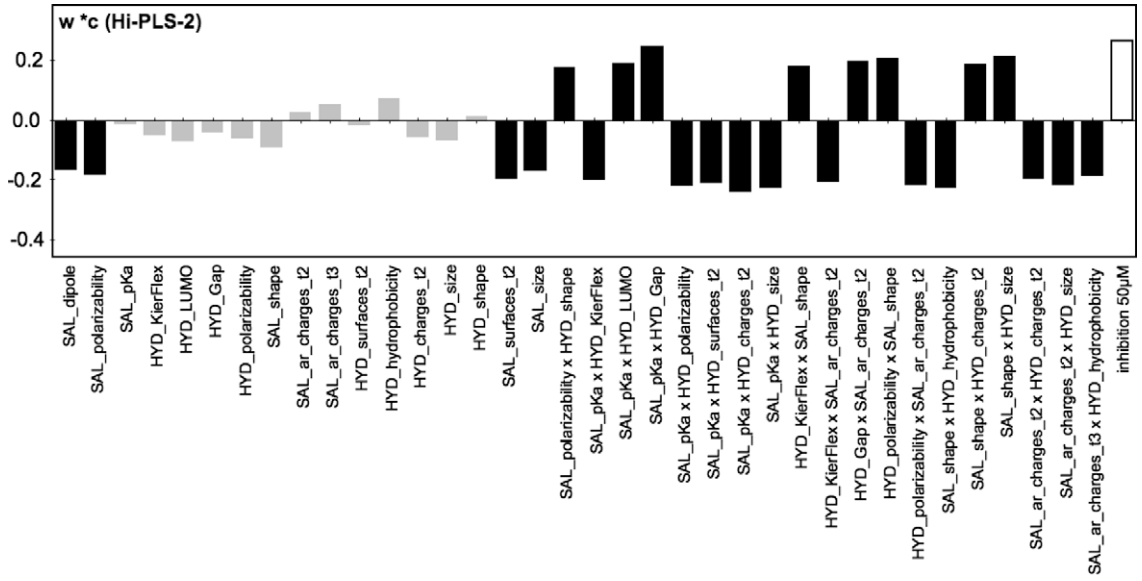

Figure 8. Loading (w*c) column plot from **Hi-PLS-2**. The loadings in black were used for interpretation. The loadings in gray could not be removed as the variables were used in non-linear terms important for the model.

Table 3
Percentage inhibition of luciferase light emission for strain YPIII-pIB102 (*yopE-luxAB*) in the presence of external test compounds **ME0257**–**ME0264** at 100, 50, 25, and 12.5 μM concentrations

ID	Structure	100 μM[a]	50 μM[a]	25 μM[a]	12.5 μM[a]	Hi-PLS-1	Hi-PLS-2	Hi-PLS-DA-1	*Chlamydia* MIC[b] (μM)	Cell viability 50 μM[a] (%)	Cell viability 25 μM[a] (%)
ME0257	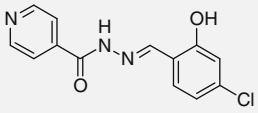	96 ± 2	84 ± 2	27 ± 5	4 ± 4	49	47	Border line active	Inactive	67 ± 4	72 ± 1
ME0258	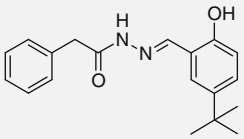	20 ± 4	26 ± 3	10 ± 2	4 ± 12	25	34	Inactive	Inactive	79 ± 3	83 ± 2
ME0259	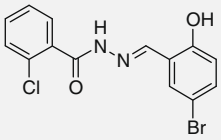	58 ± 5	38 ± 6	11 ± 3	13 ± 9	73	48	Active	50	60 ± 1	77 ± 1
ME0260	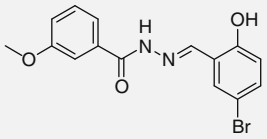	71 ± 4	44 ± 2	22 ± 4	15 ± 2	64	46	Active	25	65 ± 2	73 ± 3
ME0261	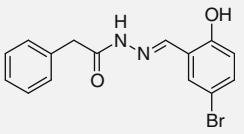	39 ± 3	26 ± 4	15 ± 7	7 ± 10	68	51	Active	50	74 ± 3	75 ± 1
ME0262	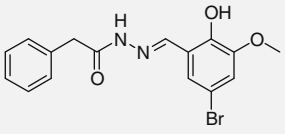	57 ± 8	22 ± 3	9 ± 7	15 ± 1	20	31	Inactive	Inactive	33 ± 1	58 ± 2
ME0263	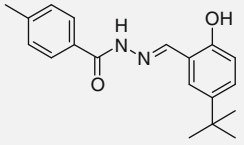	24 ± 6	17 ± 15	20 ± 6	18 ± 3	26	34	Inactive	50	79 ± 1	80 ± 4
ME0264	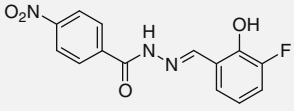	20 ± 15	28 ± 10	19 ± 7	4 ± 7	53	62	Border line active	50	72 ± 1	75 ± 2

Compounds with at least 40% inhibition at 50 μM compound concentration were defined as active. The predicted inhibition is given for **Hi-PLS-1** and **Hi-PLS-2** and the predicted class membership for **Hi-PLS-DA-1** at 50 μM compound concentration. Minimum inhibitory concentration, MIC, of *Chlamydia trachomatis* growth was tested at 50, 25, 12.5, 6.25, 3.13 μM. Compound toxicity to the host cells used for *Chlamydia* growth, HeLa 229, was tested at 50 and 25 μM. Compounds were defined as non-toxic when HeLa229 cell viability was at least 70% relative to controls.

[a] Means and standard deviations are calculated from triplicates, and experiments were reproduced on at least three separate occasions.

[b] *Chlamydia* MIC was tested in duplicates on at least three separate occasions.

T3S inhibition in *Yersinia* as well as growth inhibition of *Chlamydia*, supporting a common mode of action. There are however some differences, such as **ME0263**, that is, inhibiting *Chlamydia* growth but is inactive in the *Yersinia* assays, or **ME0257**, that is, active in *Yersinia* but unable to inhibit *Chlamydia* growth. These discrepancies could possibly be related to membrane properties that differ between *Yersinia*, *Chlamydia* and its eukaryotic host cell.

To ensure that the observed inhibition of *Chlamydia* growth was not a result of the salicylidene acylhydrazides being toxic to the infected HeLa 229 cells, cell viability was measured (Table 3). Four of the five external test set compounds, **ME0260**, **ME0261**, **ME0263**, and **ME0264,** that completely inhibited *Chlamydia* growth were not toxic to HeLa 229 cells (70% or higher cell viability compared to the DMSO control at the lowest concentrations where *Chlamydia* was inhibited). Only **ME0259** was slightly toxic (60% cell viability at 50 μM compound concentration).

2.8. Mode of action

The first detailed investigation of the salicylidene acylhydrazides as T3S inhibitors showed that the inhibition is instantaneous, reversible, and that the compounds likely act directly on the secretion machinery that span the inner and outer membranes of the bacterium.[13] The T3S syringe-like apparatus with a needle and membrane-spanning base is highly conserved while its regulation and effector proteins often are unique for the different bacterial species. The fact that the compounds inhibit T3S in *Y. pseudotuberculosis*,[13] *Salmonella enterica*,[24,25] *Shigella flexneri*,[26] enterohemorrhagic *E. coli*,[27] and *Chlamydia* spp.[23,28–30] support a direct inhibition of the T3S machinery. In contrast the intracellular pathogen *Coxiella burnetii* that utilizes a type four secretion (T4S) system was unaffected[23] and in the present study we show that the toxicity from toxins secreted by a T2S system in enterotoxigenic *E. coli* is unaffected at

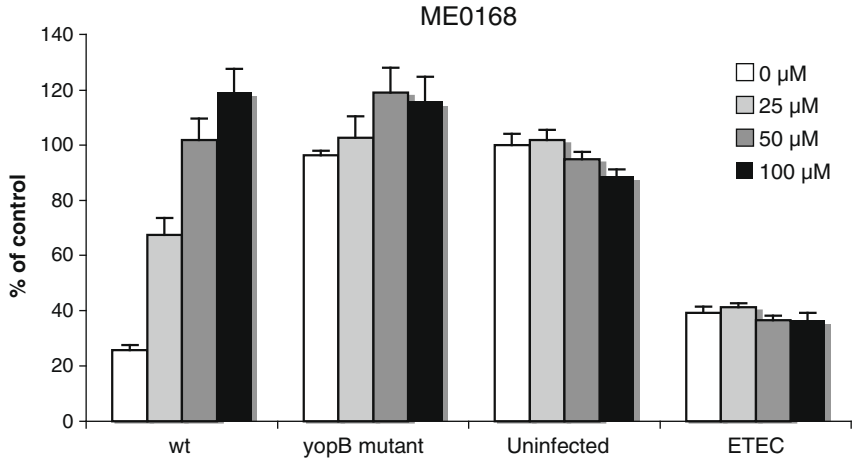

Figure 9. Infection of J774 macrophages with wild-type *Y. pseudotuberculosis*, a non-virulent yopB mutant strain of *Y. pseudotuberculosis*, and enterotoxigenic *E. coli* (ETEC) in the presence of different concentrations of **ME0168**. Macrophage viability was quantified from the fluorescence signal originating from enzymatic conversion of the reagent CalceinAM. Viability for uninfected cells corresponds to 100%. **ME0168** is non-toxic and selectively rescues macrophages infected with wild-type *Y. pseudotuberculosis*. Error bars are calculated with Gauss approximation formula.

concentrations that inhibit T3S. The T3S syringe-like machinery shows remarkable similarity to the hook-basal body of the flagellum.[5,52] The flagellum is an organelle required for bacterial motility and interestingly salicylidene acylhydrazides inhibit motility in *Y. pseudotuberculosis*[6] and *S. enterica*.[24] This further supports the hypothesis that the compounds target the conserved machinery directly. Further support comes from the finding that treatment of *S. flexneri* with a salicylidene acylhydrazide resulted in increased numbers of T3S apparatuses without needles or with shorter needles.[26] This indicates that the inhibitor blocks secretion of the needle protein component(s), the first level of protein export required for assembly of a fully functional T3S machinery. In a recent study trancriptomics were used in a comprehensive analysis of the effects of four salicylidene acylhydrazides on enterohemorrhagic *E. coli*.[27] The results showed that the compounds inhibit expression of the T3S system but it remains to be established if this effect is a result from feed-back regulation originating from inhibition of the secretion apparatus or if the compounds target a regulatory pathway.

An interesting feature of the salicylidene acylhydrazides is that they can act as trivalent ligands in complexes with metal cations and a number of complexes have been prepared and their structures determined.[53,54] Due to their chelation capacity the compounds have been investigated as therapeutic agents against iron poisoning.[55] Intracellular pathogens require iron for growth and addition of Fe^{2+} and Fe^{3+} reversed the effect of salicylidene acylhydrazides in *C. trachomatis*.[30] The observed inhibition of growth of *Chlamydia* spp. might thus be the result of iron deprivation rather than a blocked T3S system. The fact that inhibition of T3S in *Y. pseudotuberculosis* could not be abrogated by addition of iron argues otherwise.[30] Transcriptomic analysis was recently carried out in *E. coli* and showed that iron response genes were unaffected by the compounds and the *E. coli* were therefore not suffering from iron depletion.[27] A plausible explanation is that *Chlamydia* spp. utilize T3S to secure a supply of iron that enable intracellular growth.[30]

Our QSAR models and a visual comparison of active and inactive compounds reveal no clear and straightforward interpretation. It is possible that the salicylidene acylhydrazides inhibit T3S as metal complexes containing one or two compounds or that binding to the target involves a metal ion. The structural features that the QSAR models indicate as critical for activity can therefore describe properties important for a binding mode that involves the protein target and one or more metal ions. Since the compounds were evaluated in cell-based systems the QSAR models most likely also capture important global chemical features affecting, for example, permeability and metabolic stability. The fact that QSAR models could be computed and the models could be validated with an external test set in two biologically different T3S dependent pathogens strongly support a common and selective mode of action on the T3S apparatus directly or on its regulation.

3. Conclusions

Application of an SMD strategy resulted in 50 compounds and after biological evaluation three QSAR models with acceptable statistics could be established. The models differed to a large extent and predictions were therefore made in consensus. The models could correctly classify six of eight compounds in an external test set. To further establish the potential of this class of compounds a selected set of inhibitors were evaluated in cell-based infection models. It was found that compounds active in the first line assays also displayed a selective and non-toxic virulence-blocking activity. In conclusion we illustrate that the combined use of SMD, QSAR modeling, and validation with an external test set predicted in consensus is an effective and general strategy for generation of information important in the process of lead identification and optimization.

4. Experimental section

4.1. Characterization of BBs

BBs were selected manually from Aldrich, Maybridge, ABCR, Acros, and Alfa Aesar based on availability, size and chemical compatibility. For the hydrazide BBs only up to two connected ring systems were allowed and all BBs with molecular weight lower than 50 or higher than 300 were removed. In addition, BBs having more than two atoms connecting the hydrazide part and the ring system were removed. Finally BBs containing chiral centers were removed. The final sets contained 48 salicylic aldehydes (Fig. S1) and 92 hydrazides (Fig. S2). The BBs were created in MOE[56] and for the salicylic aldehydes a conformational analysis was performed using OMEGA[57] with default settings. The conformational analysis for the hydrazide BBs was performed in MOE using stochastic conformational search with default settings, except the MM iteration limit that was changed from 200 to 800. The

conformations of both BB sets were imported to MOE and the MMFF94X force field partial charges were calculated. The conformations were energy minimized in MOE using the MMFF94X force field with a root mean square gradient of 0.1. For each resulting conformation, the AM1 energy was calculated in MOE and the conformation with lowest energy for each BB was saved. The low energy conformations were then further geometry optimized using a Hartree–Fock calculation in Jaguar.[58] In Jaguar a number of descriptors (e.g., polarizability and moment of inertia) were calculated. The geometry optimized structures were imported back into MOE where atomic partial charges were assigned for each BB using AM1 calculations. A second set of descriptors was then calculated in MOE and added to the descriptors calculated in Jaguar, resulting in a total set of 70 descriptors for the salicylic aldehydes and 97 descriptors for the hydrazides. The total descriptor set for each BB set is given in Supplementary data (Tables S1 and S6).

4.2. Statistical molecular design

The design procedure is summarized in Figure 2, and explained in detail here. For the salicylic aldehydes, descriptors describing hydrophobicity (Table S2) and charges (Table S3) were grouped separately and imported to Simca 12.0.[59] Data was centered and scaled to unit variance (as was the case for all PCA and PLS models) and two local PCA models were generated to summarize the information (Table S4). There was some overlap of descriptors in both these PCA models since some descriptors described both polarity and charges. The number of significant components in all PCA models was determined by the eigenvalue of the last component (components with an normalized eigenvalue $\geq$2.0 were considered significant), cross-validation using seven cross-validation rounds as implemented in Simca 12.0,[59] and inspection of the loading plots to see that the components held unique information. Compounds with eigenvalues lower than 2.0 were accepted, as long as the other two criteria were fulfilled. The resulting PCA score vectors were combined with the ab initio descriptors, molecular weight and volume (Table S5). A new PCA model was computed to compress the data. The PCA score vectors were extracted and used as design variables in a two-layer linear DOOD, as implemented in MODDE 8.0.2.[60] The hydrazide descriptors were summarized using PCA, and the PCA score vectors were used in a second DOOD, performed in the same manner as for salicylic aldehydes. We did not have any indication about which properties of the hydrazides that could correlate with the biological activity, and therefore we did not do a block wise PCA of the BBs. The final products were selected by having both BB sets in separate columns where the BBs were in randomized order. The two columns were combined to form the first 18 virtual products. The hydrazide BB column was shifted one step downwards so that the last BB in the column became the first. The two BB columns were combined to form the second set of 18 virtual products. A second downward shift of the hydrazide BB column followed by combination with the salicylic aldehyde BB column gave the final 18 virtual products.

4.3. General assay conditions

The biological evaluation of the salicylidene acylhydrazides was performed in *Y. pseudotuberculosis* according to previously published methods[6,13] using a T3S linked luciferase reporter-gene assay (Tables 1 and 3, S9a, and S9b) and an enzymatic YopH assay (data not shown). *Y. pseudotuberculosis* serotype III strain YPIII pIB102 (*yopE-luxAB*) was grown overnight, at room temperature, in brain heart infusion (BHI) containing ethylene glycol tetraacetic acid (5 mM) and $MgCl_2$ (20 mM) for calcium depletion. The optical density of the bacteria measured at 600 nm (OD_{600}) was adjusted to 0.088–0.095 in BHI. To each well in a 96-well plate (Nunc™, flat bottom, white) bacterial solution (100 μL) was added, followed by addition of compound (1 μL DMSO solution) to give the final compound concentrations 1.56, 3.13, 6.25, 12.5, 25, 50, 100, and 200 μM. The plates were incubated on a rotary shaker for 1 h at room temperature followed by 2 h at 37 °C. After incubation, 10 μL of the bacterial suspension was transferred to new 96-well plates (Nunc™, flat bottom, transparent) containing YopH substrate mixture (90 μL, 25 mM *p*-nitro phenyl phosphate, 40 mM 2-(N-morpholino)ethanesulfonic acid, pH 5.0, and 1.6 mM dithiothreitol in MQ water) in each well. The plates were incubated at 37 °C for 15 min before NaOH (20 μL, 1 M) was added to each well to quench the reaction. The absorbance was measured at 405 nm in a microplate reader (TECAN Infinite M200). For the luciferase assay, decanal solution (50 μL, 10 μL decanal/100 mL water) was added to the first set of plates and the light emission was immediately detected with a microplate reader (TECAN Infinite M200, Gain 150, integration time of 20 ms). All liquid handling during screening were performed with a Biomek® NX^P. Experiments were run in triplicates and reproduced at least three independent times.

Growth inhibition was measured according to published protocols.[6,13] Wild-type *Y. pseudotuberculosis* pIB102 and *E. coli* DH5α were grown overnight in Luria broth (LB) at room temperature and 37 °C, respectively, followed by a dilution to an OD_{600} = 0.1 in LB medium containing 2.5 mM $CaCl_2$. To the diluted bacteria (100 μL) compound (1 μL DMSO stock solution) was added to give a final compound concentration of 50 and 100 μM. The plates were incubated in 37 °C and the absorbance was measured at 595 nm in a plate reader (SpectraMAX 340) for 23 h (Fig. S5).

4.4. Multivariate QSAR modeling

Only compounds showing a dose–response were used to establish QSAR models, since compounds could be inactive due to several reasons, like poor solubility, efflux, and inability to pass through the double bacterial cell membrane. Compounds showing luciferase signal inhibition, but lacking inhibition of the control YopH (**ME0163**, **ME0190**–**ME0193**), were excluded from all modeling. In most attempts to establish QSAR models, compound **ME0167** was predicted to have much higher inhibition than the actual experimental value. Therefore, **ME0167** was excluded from all modeling, as the poor inhibition could be due to other factors than low luciferase signal inhibition, such as efflux.

For all modeling the inhibitory values at 50 μM compound concentration was used as Y-response, since the dataset had the most even spread in biological activity at this concentration. At 100 μM concentration some compounds started to precipitate and at 25 μM concentration there were too few active compounds (i.e., more than 40% inhibition). For PLS discriminant analysis (PLS-DA) classification, salicylidene acylhydrazides were classified as active if they inhibited the luciferase light emission signal by at least 40% at 50 μM compound concentration. Two sets of training set compounds were used in the modeling, one for **Hi-PLS-DA** (**Obs_1**) and one for **Hi-PLS** (**Obs_2**) models (Table 4). **Obs_2** consisted of all compounds showing a dose–response and three

Table 4
PLS score vector sets used for **Hi-PLS-1** and **Hi-PLS-DA-1**

Score vector set[a]	Training set[b]	No. of score vectors[c]	R^2Y
SAL1	Obs_1	16	0.53
HYD1	Obs_1	16	0.27
SAL2	Obs_2	14	0.64
HYD2	Obs_2	14	0.33

[a] Set of score vectors computed from PLS models based on BBs.
[b] Training set used to compute the PLS score vectors.
[c] Number of score vectors computed.

additional inactive compounds (**ME0172**, **ME0181**, **ME0197**) that all were calculated as inactive in the models, which was not the case for all inactive compounds synthesized and tested biologically.

The salicylidene acylhydrazides with a measured biological response were disassembled into their BBs and two columns, one for each BB set, were formed. To each BB column the total descriptor sets with ab initio, MM and informatics descriptors were added (Tables S1 and S6). The descriptor matrices were imported into Simca 12.0.[59] PLS regression was made of the matrices describing salicylic aldehydes or hydrazides to the luciferase signal inhibition in such a way that all BBs were listed together with their inhibition values from the corresponding molecules the BBs were used in. Thus a BB used in three salicylidene acylhydrazides would be listed with three different inhibition values. PLS components were added until the cumulative value of R^2X reached 1.0. The PLS score vectors from each BB set were extracted and combined, forming a new data matrix consisting of all training set compounds and their score vector descriptor. The PLS score vectors were expanded with square and interaction terms. A variable selection, fully described in Supplementary data, was performed to compute the final models (Table S10 for **Hi-PLS-1** and Table S11 for **Hi-PLS-DA-1**).

The methodology used to compute **Hi-PLS-2** (using **Obs_2**) and **Hi-PLS-DA-2** (using **Obs_1**) is summarized in Figure 6 and described in detail here. Descriptors describing similar properties were grouped into six groups for the salicylic aldehydes and five for the hydrazides (Table S12). Those descriptors that could not be assigned to a group (e.g., pK_a and HOMO) were kept as independent descriptors ($X1_U$ and $X2_U$). The grouped descriptors were summarized using local PCA models, generating the score vectors $X1_1 - X1_6$ for the salicylic aldehydes and $X2_1 - X2_5$ for the hydrazides (Table S13). The PCA score vectors from the local models and the independent descriptors from both BB sets were combined (Table S14) and expanded by square and interaction terms. Following variable selection the final models could be computed (Table S15 for **Hi-PLS-2** and Table S16 for **Hi-PLS-DA-2**).

The fraction of sum of squares of Y that can be explained by one PLS component (R^2Y), was calculated as:

$$R^2Y = SS_{mod}/SS_{tot}$$

where SS_{mod} is the sum of square of the responses corrected for the mean and SS_{tot} the total sum of squares of Y corrected for the mean.

The fraction of the total variation of Y that can be predicted by one component (Q^2), as estimated by cross-validation, was calculated using seven cross-validation rounds according to:

$$Q^2 = 1 - PRESS/SS_{tot}$$

where PRESS is the predicted error sum of squares when all objects have been left out once.

Four models were computed with logit transformed response, as implemented in Simca 12.0,[59] in order to compensate for the non-normalized distribution in activity of the training set and S-shaped curvature of the experimental versus calculated luciferase signal inhibition. The logit transformed models did not differ from the non-transformed models in their predictions and interpretability. The logit transformed models are given fully in Supplementary data (p. S35 for an overview of the logit transformed models, Figs. S13–S23, and Tables S17–S22).

All PLS models were evaluated with permutation tests, using Simca 12.0,[59] where the order of the biological response was randomized using 300 permutations for each model (Figs. S7, S8, and S21–S23). The cumulative R^2 and Q^2 gave a regression line where the intercept is an estimate of the significance of the models generated.[61] A positive intercept for Q^2 would indicate that most models would be significant no matter the order of the response and thus the model would be insignificant and likely just a result of chance correlation.

4.5. Evaluation of models using an external test set

All the combinations of BBs used in the SMD were enumerated. Compounds with a DModX,[62] that is, the residual standard deviation, cutoff higher than 1.40 in the PLS models and 1.33 in the PLS-DA model were excluded. The total set was predicted in the three models and the compounds predicted as active (≥40% inhibition of luciferase light emission for **Hi-PLS-1** and **Hi-PLS-2** and class membership to the actives for **Hi-PLS-DA-1**) were recorded. The overlap between the models was then calculated, disregarding any compounds having a higher DModX than the cutoff in any of the three models.

DModX is essentially a tool to detect model outliers, but can also be used to limit the test set depending on the goal of the predictions. A compound is considered non-deviating if it has a smaller value than the critical distance, D-crit,[59] in DModX. D-crit is calculated from the F-distribution of the last component of the model in question. If the goal is to improve existing QSAR models by inclusion of a few additional compounds, then a low DModX cutoff and a wide range of biological activity might be good choices. If the aim is to find one potent inhibitor and a large synthetic effort can be put into identifying this compound, a predicted response over 90% and a DModX two or three times the D-Crit value might be wise choices. If the goal is to establish models that theoretically can predict the entire virtual set of compounds based on commercially available BBs, a new SMD could be performed using some or all of the coefficients from the QSAR model. Since QSAR models are interpolating, the SMD should in this case cover the outer domain of the virtual product space, possibly excluding extreme outliers as indicated by DModX.

4.6. *Yersinia pseudotuberculosis* and enterotoxigenic *Escherichia coli* infection of J774A Cells

The experimental procedures were essentially carried out as described before[29] with compounds **ME0165**–**ME0167**, **ME0174**, and **ME0181**. J774A cells were seeded out into 96-well plates (4×10^4 cells/well) in Dulbecco's modified Eagle's medium (DMEM) with 10% fetal calf serum (FCS) and gentamicin (3 μg/mL), grown for 24 h at 37 °C in 5% CO_2. *Y. pseudotuberculosis* wild-type pIB102 and pIB604 Δ*yopB* (translocation-deficient T3S mutant) were grown in LB medium supplemented with kanamycin (25 μg/mL) at room temperature overnight, diluted 1/10 in DMEM and incubated on a rotary shaker at room temperature 1 h and at 37 °C for 2 h. Enterotoxigenic *E. coli* (ETEC) was grown in LB medium overnight at 37 °C, diluted as above and grown at 37 °C for 3 h. The J774A cells were washed with phosphate buffered saline (PBS, 100 μL) then fresh DMEM (50 μL) containing the different compounds (**ME0165**–**ME0167**, **ME0174**, and **ME0181**, added from DMSO stock solutions) and bacteria (50 μL, OD_{600} = 0.002) were added to give 25, 50, and 100 μM final compound concentrations. The final DMSO concentration was kept below 0.5%. The plate was incubated for 14 h at 37 °C in 5% CO_2. CalceinAM (Invitrogen, 20 μL of a 6 μM solution in PBS) was added and the plate was incubated for 40 min at 37 °C in 5% CO_2. The fluorescence was measured in a microplate reader (TECAN Infinite M200) at 485/535 nm (Fig. 9 and S12) and the results were confirmed using fluorescent microscopy (data not shown). As a rescue control gentamycin (5 μg/mL) was added to the cells infected with ETEC.

4.7. Determination of minimum inhibitory concentration (MIC) for *Chlamydia trachomatis*

HeLa 229 cells cultured in 96-well microtiter plates were infected with *C. trachomatis* serovar L2 at multiplicity of infection 0.3. Compounds or solvent (DMSO final concentration 1%) were diluted in RPMI 1640 medium with supplements (10% fetal calf serum, 2 mM L-glutamine, 8 μg/mL gentamicin) and added to the infected cells one hour after infection. After 35 h incubation at 37 °C in a humidified atmosphere of 5% (v/v) CO_2/air, cells were fixed with methanol, immunostained (Pathfinder, Biorad) and examined using fluorescent microscopy at 200× magnification. All compounds were tested at 50, 25, 12.5, 6.25, and 3.13 μM and tests were performed in duplicates at least three times. Minimum inhibitory concentration was defined as the lowest tested concentration where no intracellular growth was observed.

4.8. Cell viability assay

HeLa 229 cells cultured in 96-well microtiter plates were incubated with test compounds (50 μM and 25 μM) or solvent (DMSO final concentration 1%) diluted in non-colored DMEM with supplements (0.5% fetal calf serum, 2 mM L-glutamine, 8 μg/mL gentamicin) for totally 28 h at 37 °C in a humidified atmosphere of 5% (v/v) CO_2/air. Cell viability was evaluated using a resazurin (blue and non-fluorescent, Sigma 40 μM final concentration), that is, reduced to resorufin (pink and highly fluorescent) in living cells.[63,64] Fluorescence was measured using a Tecan Safire plate reader with excitation at 535 nm and emission at 595 nm. Resazurin was added four hours prior to measurement and cell-free wells with medium and compound were used to rule out chemical reduction of resazurin by the compounds. Scoring was made relative to the DMSO control. In addition, cell viability was scored microscopically. All experiments were performed in triplicates and repeated at least three times.

4.9. General chemistry

Mass-spectra were recorded by detecting negative (ES^-) molecular ions with an electro spray Waters Micromass ZG 2000 instrument using an XTerra® MS C_{18} 5 μM 4.6 × 50 mm column and an H_2O/acetonitrile/formic acid eluent system. The same LC-system was also used for purification with a preparative XTerra® Prep MS C_{18} 5 μM 19 × 50 mm column and an H_2O/acetonitrile eluent system. Reflux reactions were performed using a Radley carousel 12 reaction station. Microwave heated reactions were performed in Emrys™ process vials (20 mL) using a SmithCreator™ microwave instrument from Biotage. ^{1}H NMR spectra were recorded in DMSO-d_6 (residual DMSO-d_5, δ_H = 2.50 ppm, as internal standard) using a 400 MHz Bruker spectrometer.

4.10. Typical procedure for the formation of salicylidene acylhydrazides

Salicylic aldehyde (0.7–1.4 mmol, 1 equiv) and hydrazide (1.4 equiv) were suspended in absolute ethanol (10 mL) and refluxed for 4 h, or heated using a microwave instrument at 155 °C for 7 min. Remaining solid was filtered off and analyzed using LC–MS. If the filtrand was impure, the filtrate and ethanol (100 mL) was added and the mixture was heated under stirring until all material was thoroughly dissolved. If the mixture could not be dissolved completely by the addition of ethanol, DMSO (2–5 mL) was added. If a heterogeneous mixture still remained, a warm filtration was performed. From the resulting solution a pure precipitate was generally formed by the addition of cold water. The precipitate was filtered off using suction filtration and washed with water. If no precipitate could be formed, the products was purified using preparative LC–MS. Compound purities, calculated from LC–UV traces, are given in Supplementary data (Table S8).

4.10.1. 4-Methyl-[1,2,3]thiadiazole-5-carboxylic acid (6-bromo-2-hydroxy-3-methoxy-benzylidene)-hydrazide (ME0150)

Two rotamers were obtained in a 1:0.73 ratio as a result of a dynamic process. ^{1}H NMR (major rotamer): δ 12.59–12.36 (m, 1H), 9.90 (s, 1H), 8.88 (s, 1H), 7.16 (d, J = 8.7 Hz, 1H), 7.01 (d, J = 8.7 Hz, 1H), 3.81 (s, 3H), 2.87 (s, 3H); ^{1}H NMR (minor rotamer): δ 12.78 (br s, 1H), 9.90 (s, 1H), 8.41 (s, 1H), 7.15 (d, J = 8.7 Hz, 1H), 7.01 (d, J = 8.7 Hz, 1H), 3.84 (s, 3H), 2.92 (s, 3H); LC–MS $[M-H^+]^-$ calcd for $[C_{12}H_{11}BrN_4O_3S]$: m/z: 368.96; found: 369.03.

4.10.2. Isonicotinic acid (6-bromo-2-hydroxy-3-methoxy-benzylidene)-hydrazide (ME0151)

^{1}H NMR: δ 12.68 (s, 1H), 12.60 (s, 1H), 9.00 (s, 1H), 8.85–8.80 (m, 2H), 7.89–7.84 (m, 2H), 7.16 (d, J = 8.7 Hz, 1H), 7.01 (d, J = 8.7 Hz, 1H), 3.81 (s, 3H); LC–MS $[M-H^+]^-$ calcd for $[C_{14}H_{12}BrN_3O_3]$: m/z: 348.00; found: 348.18.

4.10.3. Cyano-acetic acid (6-bromo-2-hydroxy-3-methoxy-benzylidene)-hydrazide (ME0152)

Two rotamers were obtained in a 1:0.45 ratio as a result of a dynamic process. ^{1}H NMR (major rotamer): δ 12.31 (br s, 1H), 12.23 (s, 1H), 8.69 (s, 1H), 7.15 (d, J = 8.7 Hz, 1H), 6.99 (d, J = 8.7 Hz, 1H), 3.89 (s, 2H), 3.80 (s, 3H); ^{1}H NMR (minor rotamer): δ 12.23 (s, 1H), 10.39 (s, 1H), 8.47 (s, 1H), 7.14 (d, J = 8.7 Hz, 1H), 6.98 (d, J = 8.7 Hz, 1H), 4.23 (s, 2H), 3.80 (s, 3H); LC–MS $[M-H^+]^-$ calcd for $[C_{11}H_{10}BrN_3O_3]$: m/z: 309.98; found: 310.06.

4.10.4. 2-Bromo-5-methoxy-benzoic acid (4-chloro-2-hydroxy-benzylidene)-hydrazide (ME0153)

Two rotamers were obtained in a 1:0.45 ratio as a result of a dynamic process. ^{1}H NMR (major rotamer): δ 12.10 (s, 1H), 11.31 (s, 1H), 8.47 (s, 1H), 7.64 (d, J = 8.2 Hz, 1H), 7.60 (d, J = 8.8 Hz, 1H), 7.17 (d, J = 3.0 Hz, 1H), 7.01–6.95 (m, 3H), 3.80 (s, 3H); ^{1}H NMR (minor rotamer): δ 12.10 (s, 1H), 10.32 (s, 1H), 8.26 (s, 1H), 7.56 (d, J = 8.7 Hz, 1H), 7.28 (d, J = 9.0 Hz, 1H), 7.04 (d, J = 3.1 Hz, 1H), 7.02 (d, J = 3.2 Hz, 1H), 6.89–6.84 (m, 2H), 3.77 (s, 3H); LC–MS $[M-H^+]^-$ calcd for $[C_{15}H_{12}BrClN_2O_3]$: m/z: 380.96; found: 381.03.

4.10.5. 4-Bromo-benzoic acid (4-chloro-2-hydroxy-benzylidene)-hydrazide (ME0154)

Two rotamers were obtained in a 1:0.11 ratio as a result of a dynamic process. ^{1}H NMR (major rotamer): δ 12.17 (s, 1H), 11.53 (s, 1H), 8.63 (s, 1H), 7.89 (d, J = 8.5 Hz, 2H), 7.77 (d, J = 8.5 Hz, 2H), 7.64 (d, J = 8.1 Hz, 1H), 7.02–6.95 (m, 2H); ^{1}H NMR (minor rotamer): δ 12.17 (s, 1H), 11.83 (s, 1H), 8.32 (br s, 1H), 7.89 (d, J = 8.5 Hz, 2H), 7.77 (d, J = 8.5 Hz, 2H), 7.70 (br s, 1H), 7.46 (br s, 1H), 6.91 (br s, 1H); LC–MS $[M-H^+]^-$ calcd for $[C_{14}H_{10}BrClN_2O_2]$: m/z: 350.95; found: 351.09.

4.10.6. Adamantan-1-yl-acetic acid (4-chloro-2-hydroxy-benzylidene)-hydrazide (ME0155)

Two rotamers were obtained in a 1:0.39 ratio as a result of a dynamic process. ^{1}H NMR (major rotamer): δ 11.52 (s, 2H), 8.33 (s, 1H), 7.55 (d, J = 8.1 Hz, 1H), 6.96 (s, 1H), 6.95–6.91 (m, 1H), 1.97 (s, 2H), 1.93 (br s, 3H), 1.70–1.53 (m, 12H); ^{1}H NMR (minor rotamer): δ 11.21 (s, 1H), 10.58 (br s, 1H), 8.19 (s, 1H), 7.64 (d, J = 8.8 Hz, 1H), 6.96 (br s, 1H), 6.95–6.91 (m, 1H), 2.40 (s, 2H), 1.93 (br s, 3H), 1.70–1.53 (m, 12H); LC–MS $[M-H^+]^-$ calcd for $[C_{19}H_{23}ClN_2O_2]$: m/z: 345.13; found: 345.26.

4.10.7. 3,4-Dimethoxy-benzoic acid (2-hydroxy-3,5-diiodo-benzylidene)-hydrazide (ME0156)

^{1}H NMR: δ 13.02 (s, 1H), 12.35 (s, 1H), 8.43 (s, 1H), 8.04 (s, 1H), 7.86 (d, J = 1.8 Hz, 1H), 7.61 (d, J = 9.0 Hz, 1H), 7.52 (s, 1H), 7.12 (d, J = 8.5 Hz, 1H), 3.85 (s, 6H); LC–MS $[M-H^+]^-$ calcd for $[C_{16}H_{14}I_2N_2O_4]$: m/z: 550.89; found: 550.99.

4.10.8. (4-Fluoro-phenoxy)-acetic acid (2-hydroxy-3,5-diiodo-benzylidene)-hydrazide (ME0157)

Two rotamers were obtained in a 1:0.22 ratio as a result of a dynamic process. ^{1}H NMR (major rotamer): δ 12.66 (s, 1H), 12.23 (s, 1H), 8.37 (s, 1H), 8.05 (d, J = 1.9 Hz, 1H), 7.85 (d, J = 1.9 Hz, 1H), 7.20–7.13 (m, 2H), 7.06–7.00 (m, 2H), 4.73 (s, 2H); ^{1}H NMR (minor rotamer): δ 11.82 (s, 1H), 10.68 (br s, 1H), 8.09 (s, 1H), 7.88 (br s, 1H), 8.05 (d, J = 1.9 Hz, 1H), 7.14–7.08 (m, 2H), 6.98–6.93 (m, 2H), 5.13 (s, 2H); LC–MS $[M-H^+]^-$ calcd for $[C_{15}H_{11}FI_2N_2O_3]$: m/z: 538.87; found: 538.98.

4.10.9. 3,5-Dichloro-benzoic acid (2-hydroxy-3,5-diiodo-benzylidene)-hydrazide (ME0158)

^{1}H NMR: δ 12.71, (br s, 2H), 8.43 (s, 1H), 8.06 (d, J = 1.9 Hz, 1H), 7.96 (d, J = 1.8 Hz, 2H), 7.92 (br s, 2H); LC–MS $[M-H^+]^-$ calcd for $[C_{14}H_8Cl_2I_2N_2O_2]$: m/z: 558.80; found: 558.89.

4.10.10. 3,4,5-Trimethoxy-benzoic acid (2-hydroxy-3-methoxy-benzylidene)-hydrazide (ME0159)

^{1}H NMR: δ 11.94 (s, 1H), 10.93 (s, 1H), 8.66 (s, 1H), 7.26 (s, 2H), 7.16 (d, J = 7.7 Hz, 1H), 7.03 (d, J = 7.6 Hz, 1H), 6.87 (t, J = 7.9 Hz, 1H), 3.86 (s, 6H), 3.81 (s, 3H), 3.73 (s, 3H); LC–MS $[M-H^+]^-$ calcd for $[C_{18}H_{20}N_2O_6]$: m/z: 359.12; found: 359.20.

4.10.11. 2-Nitro-benzoic acid (2-hydroxy-3-methoxy-benzylidene)-hydrazide (ME0160)

Two rotamers were obtained in a 1:0.70 ratio as a result of a dynamic process. The phenol protons were exchange broadened. ^{1}H NMR (major rotamer): δ 9.28 (s, 1H), 8.31 (s, 1H), 8.21–8.17 (m, 1H), 7.91–7.85 (m, 1H), 7.82–7.72 (m, 1H), 7.69–7.65 (m, 1H), 6.94–6.90 (m, 1H), 6.77–6.73 (m, 1H), 6.72–6.66 (m, 1H), 3.76 (s, 3H); ^{1}H NMR (minor rotamer): δ 10.51 (s, 1H), 8.50 (s, 1H), 8.17–8.13 (m, 1H), 7.91–7.85 (m, 1H), 7.82–7.72 (m, 2H), 7.23–7.18 (m, 1H), 7.07–7.02 (m, 1H), 6.90–6.84 (m, 1H), 3.82 (s, 3H)); LC–MS $[M-H^+]^-$ calcd for $[C_{15}H_{13}N_3O_5]$: m/z: 314.08; found: 314.20.

4.10.12. 3-(4-Hydroxy-phenyl)-propionic acid (2,4,6-trihydroxy-benzylidene)-hydrazide (ME0161)

Two rotamers were obtained in a 1:0.19 ratio as a result of a dynamic process. ^{1}H NMR (major rotamer): δ 11.32 (s, 1H), 10.95 (s, 2H), 9.76 (s, 1H), 9.15 (s, 1H), 8.46 (s, 1H), 7.11–6.94 (m, 2H), 6.76–6.60 (m, 2H), 5.81 (s, 2H), 2.84–2.71 (m, 2H), 2.45–2.36 (m, 2H); ^{1}H NMR (minor rotamer): δ 11.11 (s, 1H), 10.52 (s, 2H), 9.76 (s, 1H), 9.15 (s, 1H), 8.36 (s, 1H), 7.11–6.94 (m, 2H), 6.76–6.60 (m, 2H), 5.82 (s, 2H), 2.84–2.71 (m, 2H), 2.69–2.63 (m, 2H); LC–MS $[M-H^+]^-$ calcd for $[C_{16}H_{16}N_2O_5]$: m/z: 315.10; found: 315.18.

4.10.13. 3-Chloro-benzo[*b*]thiophene-2-carboxylic acid (2,4,6-trihydroxy-benzylidene)-hydrazide (ME0162)

Two rotamers were obtained in a 1:0.20 ratio as a result of a dynamic process. ^{1}H NMR (major rotamer): δ 12.03 (2, 1H), 11.01 (s, 2H), 9.89 (s, 1H), 8.77 (s, 1H), 8.20–8.12 (m, 1H), 7.98–7.87 (m, 1H), 7.66–7.56 (m, 2H), 5.85 (s, 2H); ^{1}H NMR (minor rotamer): δ 12.12 (br s, 1H), 10.20 (s, 2H), 9.89 (s, 1H), 8.51 (s, 1H), 8.20–8.12 (m, 1H), 7.98–7.87 (m, 1H), 7.66–7.56 (m, 2H), 5.72 (s, 2H); LC–MS $[M-H^+]^-$ calcd for $[C_{16}H_{11}ClN_2O_4S]$: m/z: 361.00; found: 361.08.

4.10.14. 2-Oxo-2-[*N*′-(2,4,6-trihydroxy-benzylidene)-hydrazino]-acetamide (ME0163)

^{1}H NMR: δ 12.26 (s, 1H), 11.02 (s, 2H), 9.85 (s, 1H), 8.87 (s, 1H), 8.22 (s, 1H), 7.91 (s, 1H), 5.81 (s, 2H); LC–MS $[M-H^+]^-$ calcd for $[C_9H_9N_3O_5]$: m/z: 238.04; found: 238.17.

4.10.15. 3-Trifluoromethyl-benzoic acid (3-fluoro-2-hydroxy-benzylidene)-hydrazide (ME0164)

Two rotamers were obtained although the minor rotamer was not assigned due to a ratio of less than 0.02:1. The amide and phenol protons were exchange broadened. ^{1}H NMR: δ 8.68 (s, 1H), 8.28 (s, 1H), 8.25 (d, J = 8.0 Hz, 1H), 7.77 (d, J = 8.0 Hz, 1H), 7.81 (t, J = 7.8 Hz, 1H), 7.43 (d, J = 7.8 Hz, 1H), 7.34–7.25 (m, 1H), 6.97–6.89 (m, 1H); LC–MS $[M-H^+]^-$ calcd for $[C_{15}H_{10}F_4N_2O_2]$: m/z: 325.06; found: 325.19.

4.10.16. (4-Nitro-phenoxy)-acetic acid (3-fluoro-2-hydroxy-benzylidene)-hydrazide (ME0165)

Two rotamers were obtained in a 1:0.92 ratio as a result of a dynamic process. ^{1}H NMR (major rotamer): δ 11.72 (s, 1H), 11.29 (br s, 1H), 8.33 (s, 1H), 8.20 (d, J = 9.3 Hz, 2H), 7.57 (d, J = 7.9 Hz, 1H), 7.16 (d, J = 9.3 Hz, 2H), 7.31–7.24 (m, 1H), 6.94–6.83 (m, 1H), 5.34 (s, 2H); ^{1}H NMR (minor rotamer): δ 11.98 (br s, 1H), 10.22 (br s, 1H), 8.56 (s, 1H), 8.25 (d, J = 9.2 Hz, 2H), 7.39 (d, J = 7.9 Hz, 1H), 7.22 (d, J = 9.2 Hz, 2H), 7.31–7.24 (m, 1H), 6.94–6.83 (m, 1H), 4.91 (s, 2H); LC–MS $[M-H^+]^-$ calcd for $[C_{15}H_{12}FN_3O_5]$: m/z: 332.07; found: 332.15.

4.10.17. 3-Methoxy-benzoic acid (3-fluoro-2-hydroxy-benzylidene)-hydrazide (ME0166)

^{1}H NMR: δ 12.20 (s, 1H), 11.61 (s, 1H), 8.66 (s, 1H), 7.53 (d, J = 7.7 Hz, 1H), 7.49 (d, J = 2.3 Hz, 1H), 7.46 (d, J = 7.8 Hz, 1H), 7.39 (d, J = 7.8 Hz, 1H), 7.19 (dd, J = 8.0 Hz, J = 1.6 Hz, 1H), 7.31–7.26 (m, 1H), 6.96–6.87 (m, 1H), 3.84 (s, 1H); LC–MS $[M-H^+]^-$ calcd for $[C_{15}H_{13}FN_2O_3]$: m/z: 287.08; found: 287.22.

4.10.18. 4-Methyl-[1,2,3]thiadiazole-5-carboxylic acid (3-chloro-5-fluoro-2-hydroxy-benzylidene)-hydrazide (ME0167)

Two rotamers were obtained in a 1:0.10 ratio as a result of a dynamic process. ^{1}H NMR (major rotamer): δ 12.39 (s, 1H), 10.57 (s, 1H), 8.46 (s, 1H), 7.92 (d, J = 2.4 Hz, 1H), 7.46 (dd, J = 8.7 Hz, J = 2.4 Hz, 1H), 6.91 (d, J = 8.8 Hz, 1H), 2.97 (s, 3H); ^{1}H NMR (minor rotamer): δ 12.39 (s, 1H), 10.97 (s, 1H), 8.55 (s, 1H), 7.84–7.80 (m, 1H), 7.46 (dd, J = 8.7 Hz, J = 2.4 Hz, 1H), 6.91 (d, J = 8.8 Hz, 1H), 2.84 (s, 3H); LC–MS $[M-H^+]^-$ calcd for $[C_{11}H_8ClFN_4O_2S]$: m/z: 338.95; found: 339.05.

4.10.19. Isonicotinic acid (5-bromo-2-hydroxy-benzylidene)-hydrazide (ME0168)

Two rotamers were obtained in a 1:0.10 ratio as a result of a dynamic process. ^{1}H NMR (major rotamer): δ 12.35 (s, 1H), 11.12 (s, 1H), 8.88–8.70 (m, 2H), 8.65 (s, 1H), 7.92–7.75 (m, 3H), 7.44 (dd, J = 8.7 Hz, J = 2.1 Hz, 1H), 6.91 (d, J = 8.7 Hz, 1H); ^{1}H NMR (minor rotamer): δ 12.08 (br s, 1H), 10.31 (br s, 1H), 8.88–8.70 (m, 2H), 8.31 (s, 1H), 7.92–7.75 (m, 1H), 7.63 (br s, 2H), 7.35 (d, J = 7.9 Hz, 1H), 6.83 (d, J = 8.9 Hz, 1H); LC–MS $[M-H^+]^-$ calcd for $[C_{13}H_{10}BrN_3O_2]$: m/z: 317.99; found: 318.01.

4.10.20. Cyano-acetic acid (5-bromo-2-hydroxy-benzylidene)-hydrazide (ME0169)

Two rotamers were obtained in a 1:0.36 ratio as a result of a dynamic process. The phenol and amide protons were exchange broadened. ^{1}H NMR (major rotamer): δ 8.23 (s, 1H), 7.85 (d, J = 2.5 Hz, 1H), 7.38 (dd, J = 8.7 Hz, J = 2.5 Hz, 1H), 6.91–6.83 (m, 1H), 4.24 (s, 2H); ^{1}H NMR (minor rotamer): δ 8.36 (s, 1H), 7.77

(br s, 1H), 7.45–7.40 (m, 1H), 6.91–6.83 (m, 1H), 3.82 (s, 2H); LC–MS $[M-H^+]^-$ calcd for $[C_{10}H_8BrN_3O_2]$: *m/z*: 279.97; found: 280.10.

4.10.21. 2-Bromo-5-methoxy-benzoic acid (5-*tert*-butyl-2-hydroxy-benzylidene)-hydrazide (ME0170)

Two rotamers were obtained in a 1:0.47 ratio as a result of a dynamic process. ^{1}H NMR (major rotamer): δ 12.06 (s, 1H), 10.82 (s, 1H), 8.49 (s, 1H), 7.60 (d, J=8.8 Hz, 1H), 7.57–7.52 (m, 1H), 7.35 (dd, J = 8.6 Hz, J = 2.4 Hz, 1H), 7.17 (d, J = 3.0 Hz, 1H), 7.02 (d, J = 3.1 Hz, 1H), 6.87 (d, J = 8.6 Hz, 1H), 3.81 (s, 3H), 1.27 (s, 9H); ^{1}H NMR (minor rotamer): δ 12.06 (s, 1H), 9.64 (s, 1H), 8.24 (s, 1H), 7.57–7.52 (m, 1H), 7.31 (d, J = 2.4 Hz, 1H), 7.23 (dd, J = 8.6 Hz, J = 2.4 Hz, 1H), 7.04 (d, J = 3.0 Hz, 1H), 6.98 (d, J = 8.8 Hz, J = 3.1 Hz, 1H), 6.72 (d, J = 8.6 Hz, 1H), 3.77 (s, 3H), 1.17 (s, 9H); LC–MS $[M-H^+]^-$ calcd for $[C_{19}H_{21}BrN_2O_3]$: *m/z*: 403.06; found: 403.18.

4.10.22. 4-Bromo-benzoic acid (5-*tert*-butyl-2-hydroxy-benzylidene)-hydrazide (ME0171)

Two rotamers were obtained in a 1:0.04 ratio as a result of a dynamic process. ^{1}H NMR (major rotamer): δ 12.13 (s, 1H), 11.00 (s, 1H), 8.65 (s, 1H), 7.89 (d, J = 8.5 Hz, 2H), 7.77 (d, J = 8.5 Hz, 2H), 7.52 (d, J = 2.3 Hz, 1H), 7.35 (dd, J = 8.6 Hz, J = 2.4 Hz, 1H), 6.87 (d, J = 8.6 Hz, 1H), 1.28 (s, 9H); ^{1}H NMR (minor rotamer): δ 11.83 (br s, 1H), 9.81 (br s, 1H), 8.31 (s, 1H), 7.74–7.64 (m, 4H), 7.45 (br s, 1H), 7.26 (br s, 1H), 6.79 (br s, 1H), 1.21 (s, 9H); LC–MS $[M-H^+]^-$ calcd for $[C_{18}H_{19}BrN_2O_2]$: *m/z*: 373.05; found: 373.06.

4.10.23. Adamantan-1-yl-acetic acid (5-*tert*-butyl-2-hydroxy-benzylidene)-hydrazide (ME0172)

Two rotamers were obtained in a 1:0.34 ratio as a result of a dynamic process. ^{1}H NMR (major rotamer): δ 11.45 (br s, 1H), 11.00 (br s, 1H), 8.35 (s, 1H), 7.46 (d, J = 2.4 Hz, 1H), 7.31 (dd, J = 8.6 Hz, J = 2.5 Hz, 1H), 6.89–6.77 (m, 1H), 1.97 (s, 2H), 1.93 (br s, 3H), 1.78–1.52 (m, 12H), 1.26 (s, 9H); ^{1}H NMR (minor rotamer): δ 11.19 (br s, 1H), 9.93 (br s, 1H), 8.19 (s, 1H), 7.65 (d, J = 2.4 Hz, 1H), 7.26 (dd, J = 8.6 Hz, J = 2.5 Hz, 1H), 6.89–6.77 (m, 1H), 2.41 (s, 2H), 1.93 (br s, 3H), 1.78–1.52 (m, 12H), 1.25 (s, 9H); LC–MS $[M-H^+]^-$ calcd for $[C_{23}H_{32}N_2O_2]$: *m/z*: 367.24; found: 367.28.

4.10.24. 3,4-Dimethoxy-benzoic acid (3-chloro-5-fluoro-2-hydroxy-benzylidene)-hydrazide (ME0173)

^{1}H NMR: δ 12.28 (s, 2H), 8.57 (s, 1H), 7.61 (d, J = 8.3 Hz, 1H), 7.55–7.44 (m, 3H), 7.12 (d, J = 8.5 Hz, 1H), 3.85 (s, 6H); LC–MS $[M-H^+]^-$ calcd for $[C_{16}H_{14}ClFN_2O_4]$: *m/z*: 351.05; found: 351.10.

4.10.25. 3-(4-Fluoro-phenyl)-propionic acid (3-chloro-5-fluoro-2-hydroxy-benzylidene)-hydrazide (ME0174)

Two rotamers were obtained in a 1:0.52 ratio as a result of a dynamic process. The phenol and amide protons were exchange broadened. ^{1}H NMR (major rotamer): δ 8.52 (s, 1H), 7.62–7.40 (m, 2H), 7.26–6.91 (m, 4H), 4.72 (s, 2H); ^{1}H NMR (minor rotamer): δ 8.27 (s, 1H), 7.62–7.40 (m, 2H), 7.26–6.91 (m, 4H), 5.14 (s, 2H); LC–MS $[M-H^+]^-$ calcd for $[C_{16}H_{13}ClF_2N_2O_2]$: *m/z*: 339.03; found: 339.12.

4.10.26. 3,5-Dichloro-benzoic acid (3-chloro-5-fluoro-2-hydroxy-benzylidene)-hydrazide (ME0175)

^{1}H NMR: δ 12.44 (br s, 1H), 12.06 (br s, 1H), 8.58 (s, 1H), 7.97 (d, J = 1.9 Hz, 2H), 7.92 (t, J = 1.9 Hz, 1H), 7.55–7.50 (m, 2H); LC–MS $[M-H^+]^-$ calcd for $[C_{14}H_8Cl_3FN_2O_2]$: *m/z*: 358.95; found: 359.04.

4.10.27. 3,4,5-Trimethoxy-benzoic acid (3,5-dichloro-2-hydroxy-benzylidene)-hydrazide (ME0176)

^{1}H NMR: δ 12.45 (br s, 1H), 12.37 (br s, 1H), 8.57 (s, 1H), 7.65 (d, J = 2.4 Hz, 1H), 7.62 (d, J = 2.4 Hz, 1H), 7.28 (s, 2H), 3.87 (s, 6H), 3.74 (s, 3H); LC–MS $[M-H^+]^-$ calcd for $[C_{17}H_{16}Cl_2N_2O_5]$: *m/z*: 397.03; found: 397.10.

4.10.28. 2-Nitro-benzoic acid (3,5-dichloro-2-hydroxy-benzylidene)-hydrazide (ME0177)

Two rotamers were obtained in a 1:0.72 ratio as a result of a dynamic process. ^{1}H NMR (major rotamer): δ 12.65 (br s, 1H), 12.35 (s, 1H), 8.43 (s, 1H), 8.18 (d, J = 8.0 Hz, 1H), 7.94–7.87 (m, 1H), 7.82 (d, J = 7.3 Hz, 2H), 7.72–7.68 (m, 1H), 7.22 (d, J = 7.2 Hz, 1H); ^{1}H NMR (minor rotamer): δ 12.13 (br s, 1H), 10.23 (br s, 1H), 8.26 (s, 1H), 8.22 (d, J = 8.1 Hz, 1H), 7.94–7.87 (m, 1H), 7.81–7.77 (m, 1H), 7.72–7.68 (m, 1H), 7.65 (d, J = 2.2 Hz, 1H), 7.53 (d, J = 2.1 Hz, 1H); LC–MS $[M-H^+]^-$ calcd for $[C_{14}H_9Cl_2N_3O_4]$: *m/z*: 351.99; found: 352.15.

4.10.29. 3-(4-Hydroxy-phenyl)-propionic acid (2-hydroxy-4-methoxy-benzylidene)-hydrazide (ME0178)

Two rotamers were obtained in a 1:0.40 ratio as a result of a dynamic process. ^{1}H NMR (major rotamer): δ 11.49 (br s, 1H), 11.45 (s, 1H), 9.15 (s, 1H), 8.23 (s, 1H), 7.37 (d, J = 8.6 Hz, 1H), 7.06–6.99 (m, 2H), 6.69–6.64 (m, 2H), 6.49–6.47 (m, 1H), 6.46 (d, J = 2.3 Hz, 1H), 3.76 (s, 3H), 2.81–2.74 (m, 2H), 2.47–2.41 (m, 2H); ^{1}H NMR (minor rotamer): δ 11.11 (s, 1H), 10.31 (br s, 1H), 9.15 (s, 1H), 8.15 (s, 1H), 7.48 (d, J = 8.6 Hz, 1H), 7.06–6.99 (m, 2H), 6.69–6.64 (m, 2H), 6.50 (d, J = 2.4 Hz, 1H), 6.43 (d, J = 2.3 Hz, 1H), 3.73 (s, 3H), 2.81–2.74 (m, 4H); LC–MS $[M-H^+]^-$ calcd for $[C_{17}H_{18}N_2O_4]$: *m/z*: 313.12; found: 313.20.

4.10.30. 3-Chloro-benzo[*b*]thiophene-2-carboxylic acid (2-hydroxy-4-methoxy-benzylidene)-hydrazide (ME0179)

Two rotamers were obtained in a 1:0.33 ratio as a result of a dynamic process. ^{1}H NMR (major rotamer): δ 12.07 (s, 1H), 11.30 (s, 1H), 8.56 (s, 1H), 8.21–8.10 (m, 1H), 7.98–7.91 (m, 1H), 7.68–7.58 (m, 2H), 7.50 (d, J = 8.5 Hz, 1H), 6.57–6.45 (m, 2H), 3.79 (s, 3H); ^{1}H NMR (minor rotamer): δ 12.07 (s, 1H), 10.14 (s, 1H), 8.34 (s, 1H), 8.21–8.10 (m, 1H), 7.98–7.91 (m, 1H), 7.68–7.58 (m, 2H), 7.55 (d, J = 9.1 Hz, 1H), 6.57–6.45 (m, 1H), 6.40 (br s, 1H), 3.72 (s, 3H); LC–MS $[M-H^+]^-$ calcd for $[C_{17}H_{13}ClN_2O_3S]$: *m/z*: 359.02; found: 359.10.

4.10.31. 2-[*N*′-(2-Hydroxy-4-methoxy-benzylidene)-hydrazino]-2-oxo-acetamide (ME0180)

^{1}H NMR: δ 12.29 (s, 1H), 11.39 (s, 1H), 8.64 (s, 1H), 8.26 (s, 1H), 7.95 (s, 1H), 7.37 (d, J = 8.6 Hz, 1H), 6.52 (dd, J = 8.5 Hz, J = 2.4 Hz, 1H), 6.48 (d, J = 2.4 Hz, 1H), 3.77 (s, 3H); LC–MS $[M-H^+]^-$ calcd for $[C_{10}H_{11}N_3O_4]$: *m/z*: 236.06; found: 236.21.

4.10.32. 3-Trifluoromethyl-benzoic acid (3,5-di-*tert*-butyl-2-hydroxy-benzylidene)-hydrazide (ME0181)

^{1}H NMR: δ 12.40 (s, 1H), 12.20 (s, 1H), 8.60 (s, 1H), 8.28 (s, 1H), 8.25 (d, J = 7.9 Hz, 1H), 8.01 (d, J = 7.8 Hz, 1H), 7.83 (t, J = 7.8 Hz, 1H), 7.33 (d, J = 2.2 Hz, 1H), 7.25 (d, J = 2.2 Hz, 1H), 1.42 (s, 9H), 1.29 (s, 9H); LC–MS $[M-H^+]^-$ calcd for $[C_{23}H_{27}F_3N_2O_2]$: *m/z*: 419.19; found: 419.25.

4.10.33. (4-Nitro-phenoxy)-acetic acid (3,5-di-*tert*-butyl-2-hydroxy-benzylidene)-hydrazide (ME0182)

Two rotamers were obtained in a 1:0.28 ratio as a result of a dynamic process. ^{1}H NMR (major rotamer): δ 12.11 (br s, 1H), 11.97 (br s, 1H), 8.46 (s, 1H), 8.25 (d, J = 9.1 Hz, 2H), 7.30 (s, 1H), 7.23 (s, 1H), 7.22 (d, J = 9.2 Hz, 2H), 4.92 (s, 2H), 1.39 (s, 9H), 1.28 (s, 9H); ^{1}H NMR (minor rotamer): δ 12.11 (br s, 1H), 10.46 (s, 1H), 8.46 (s, 1H), 8.20 (d, J = 9.5 Hz, 2H), 8.19 (s, 1H), 7.30 (s, 1H), 7.18 (d, J = 9.2 Hz, 2H), 5.34 (s, 2H), 1.39 (s, 9H), 1.28 (s, 9H); LC–MS $[M-H^+]^-$ calcd for $[C_{23}H_{29}N_3O_5]$: *m/z*: 426.20; found: 426.25.

4.10.34. 3-Methoxy-benzoic acid (3,5-di-*tert*-butyl-2-hydroxy-benzylidene)-hydrazide (ME0183)

^{1}H NMR: δ 12.27 (s, 1H), 12.16 (s, 1H), 8.58 (s, 1H), 7.52 (d, J = 7.7 Hz, 1H), 7.48 (t, J = 7.7 Hz, 1H), 7.47 (d, J = 7.7 Hz, 1H), 7.32 (d, J = 2.1 Hz, 1H), 7.22 (d, J = 2.2 Hz, 1H), 7.22–7.17 (m, 1H), 3.85 (s, 3H), 1.42 (s, 9H), 1.29 (s, 9H); LC–MS $[M-H^+]^-$ calcd for $[C_{23}H_{30}N_2O_3]$: *m/z*: 381.22; found: 381.29.

4.10.35. 3-Trifluoromethyl-benzoic acid (2-hydroxy-3,5-dimethoxy-benzylidene)-hydrazide (ME0184)

Two rotamers were obtained in a 1:0.09 ratio as a result of a dynamic process. ^{1}H NMR (major rotamer): δ 12.18 (s, 1H), 10.03 (s, 1H), 8.70 (s, 1H), 8.28 (s, 1H), 8.24 (d, J = 2.8 Hz, 1H), 4.87 (s, 2H), 3.79 (s, 3H), 3.72 (s, 3H); ^{1}H NMR (minor rotamer): δ 11.94 (s, 1H), 10.03 (s, 1H), 8.90 (s, 1H), 8.42 (s, 1H), 8.16 (br s, 1H), 8.08 (d, J = 8.0 Hz, 1H), 7.92 (br s, 1H), 6.59 (br s, 1H), 6.55 (br s, 1H), 3.78 (s, 3H), 3.61 (s, 3H); LC–MS $[M-H^+]^-$ calcd for $[C_{17}H_{15}F_3N_2O_4]$: *m/z*: 367.09; found: 367.11.

4.10.36. Isonicotinic acid (2-hydroxy-3-methoxy-5-nitro-benzylidene)-hydrazide (ME0185)

Two rotamers were obtained in a 1:0.08 ratio as a result of a dynamic process. The phenol and amide protons were exchange broadened. ^{1}H NMR (major rotamer): δ 8.84–8.79 (m, 2H), 8.79 (s, 1H), 8.31–8.27 (m, 1H), 7.87–7.82 (m, 2H), 7.81–7.77 (m, 1H), 3.97 (s, 3H); ^{1}H NMR (minor rotamer): δ 8.77–8.68 (m, 2H), 8.42 (br s, 1H), 7.93 (br s, 1H), 7.72 (br s, 1H), 7.65 (br s, 2H), 3.94 (s, 3H); LC–MS $[M-H^+]^-$ calcd for $[C_{14}H_{12}N_4O_5]$: *m/z*: 315.07; found: 315.15.

4.10.37. Cyano-acetic acid (2-hydroxy-3-methoxy-5-nitro-benzylidene)-hydrazide (ME0186)

Two rotamers were obtained in a 1:0.40 ratio as a result of a dynamic process. The phenol protons were exchange broadened. ^{1}H NMR (major rotamer): δ 11.87 (s, 1H), 8.33 (s, 1H), 8.25–8.19 (m, 1H), 7.74 (d, J = 2.6 Hz, 1H), 4.26 (s, 2H), 3.96 (s, 3H); ^{1}H NMR (minor rotamer): δ 11.87 (s, 1H), 8.48 (s, 1H), 8.25–8.19 /m, 1H), 7.76 (d, J = 2.6 Hz, 1H), 3.95 (s, 3H), 3.85 (s, 2H); LC–MS $[M-H^+]^-$ calcd for $[C_{11}H_{10}N_4O_5]$: *m/z*: 277.06; found: 277.18.

4.10.38. 2-Bromo-5-methoxy-benzoic acid (2-hydroxy-3,5-dinitro-benzylidene)-hydrazide (ME0187)

Two rotamers were obtained in a 1:0.32 ratio as a result of a dynamic process. ^{1}H NMR (major rotamer): δ 12.57 (br s, 1H), 12.37 (s, 1H), 8.81 (d, J = 2.9 Hz, 1H), 8.76 (d, J = 2.9 Hz, 1H), 8.66 (s, 1H), 7.62 (d, J = 8.9 Hz, 1H), 7.20 (d, J = 3.0 Hz, 1H), 7.08–7.02 (m, 1H), 3.81 (s, 3H); ^{1}H NMR (minor rotamer): δ 12.57 (br s, 1H), 12.37 (s, 1H), 8.65 (d, J = 2.9 Hz, 1H), 8.43 (s, 1H), 8.39 (d, J = 2.9 Hz, 1H), 7.59 (d, J = 8.8 Hz, 1H), 7.08–7.02 (m, 1H), 7.01 (d, J = 3.1 Hz, 1H), 3.79 (s, 3H); LC–MS $[M-H^+]^-$ calcd for $[C_{15}H_{11}BrN_4O_7]$: *m/z*: 436.97; found: 436.97.

4.10.39. 4-Bromo-benzoic acid (2-hydroxy-3,5-dinitro-benzylidene)-hydrazide (ME0188)

The amide and phenol protons were exchange broadened. ^{1}H NMR: δ 8.80 (d, J = 2.7 Hz, 1H), 8.79 (s, 1H), 8.74 (d, J = 2.7 Hz, 1H), 7.91 (d, J = 8.4 Hz, 2H), 7.78 (d, J = 8.4 Hz, 2H); LC–MS $[M-H^+]^-$ calcd for $[C_{14}H_9BrN_4O_6]$: *m/z*: 406.96; found: 406.93.

4.10.40. Adamantan-1-yl-acetic acid (2-hydroxy-3,5-dinitro-benzylidene)-hydrazide (ME0189)

Two rotamers were obtained in a 1:0.18 ratio as a result of a dynamic process. The phenol protons were exchange broadened. ^{1}H NMR (major rotamer): δ 12.02 (s, 1H), 8.76 (d, J = 2.8 Hz, 1H), 8.77 (d, J = 2.8 Hz, 1H), 8.53 (s, 1H), 2.03 (s, 2H), 1.94 (br s, 3H), 1.74–1.53 (m, 12H); ^{1}H NMR (minor rotamer): δ 11.43 (s, 1H), 8.65 (d, J = 2.9 Hz, 1H), 8.59 (d, J = 2.9 Hz, 1H), 8.30 (s, 1H), 2.44 (s, 2H), 1.94 (br s, 3H), 1.74–1.53 (m, 12H); LC–MS $[M-H^+]^-$ calcd for $[C_{19}H_{22}N_4O_6]$: *m/z*: 401.14; found: 401.19.

4.10.41. 3,4-Dimethoxy-benzoic acid (4-diethylamino-2-hydroxy-benzylidene)-hydrazide (ME0190)

^{1}H NMR: δ 11.63 (s, 1H), 11.51 (s, 1H), 8.41 (s, 1H), 7.55 (dd, J = 8.3 Hz, J = 1.9 Hz, 1H), 7.48 (d, J = 1.9 Hz), 1H), 7.18 (d, J = 8.8 Hz, 1H), 7.08 (d, J = 8.5 Hz, 1H), 6.27 (dd, J = 8.7 Hz, J = 2.3 Hz, 1H), 6.12 (d, J = 2.3 Hz, 1H), 3.83 (s, 3H), 3.83 (s, 3H), 3.36 (q, J = 7.0 Hz, 4H), 1.11 (t, J = 7.0 Hz, 6H); LC–MS $[M-H^+]^-$ calcd for $[C_{20}H_{25}N_3O_4]$: *m/z*: 370.17; found: 370.28.

4.10.42. (4-Fluoro-phenoxy)-acetic acid (4-diethylamino-2-hydroxy-benzylidene)-hydrazide (ME0191)

Two rotamers were obtained in a 1:0.34 ratio as a result of a dynamic process. ^{1}H NMR (major rotamer): δ 11.45 (br s, 1H), 11.20 (s, 1H), 8.33 (s, 1H), 7.20–7.07 (m, 3H), 7.06–6.99 (m, 2H), 6.28–6.23 (m, 1H), 6.13–6.08 (m, 1H), 4.62 (s, 2H), 3.39–3.26 (m, 4H), 1.10 (t, J = 7.0 Hz, 6H); ^{1}H NMR (minor rotamer): δ 11.20 (s, 1H), 9.83 (br s, 1H), 8.10 (s, 1H), 7.36 (d, J = 8.8 Hz, 1H), 7.20–7.07 (m, 2H), 6.96–6.89 (m, 2H), 6.25–6.21 (m, 1H), 6.13–6.08 (m, 1H), 5.01 (s, 2H), 3.39–3.26 (m, 4H), 1.10 (t, J = 7.0 Hz, 6H); LC–MS $[M-H^+]^-$ calcd for $[C_{19}H_{22}FN_3O_3]$: *m/z*: 358.15; found: 358.23.

4.10.43. 3,5-Dichloro-benzoic acid (4-diethylamino-2-hydroxy-benzylidene)-hydrazide (ME0192)

Two rotamers were obtained in a 1:0.03 ratio as a result of a dynamic process. Due to the small integrals of the minor rotamer, the amide proton could not be identified. ^{1}H NMR (major rotamer): δ 11.92 (s, 1H), 11.25 (s, 1H), 8.42 (s, 1H), 7.93 (d, J = 1.8 Hz, 2H), 7.87–7.83 (m, 1H), 7.23 (d, J = 8.8 Hz, 1H), 6.27 (dd, J = 8.8 Hz, J = 2.2 Hz, 1H), 6.12 (d, J = 2.1 Hz, 1H), 3.36 (q, J = 7.0 Hz, 4H), 1.10 (t, J = 7.0 Hz, 6H); ^{1}H NMR (minor rotamer): δ 9.81 (s, 1H), 8.14 (s, 1H), 7.78 (br s, 1H), 7.71 (br s, 2H), 7.15 (d, J = 8.8 Hz, 1H), 6.21 (d, J = 9.5 Hz, 1H), 6.06 (br s, 1H), 3.47–3.40 (m, 4H), 1.05 (t, J = 7.0 Hz, 6H); LC–MS $[M-H^+]^-$ calcd for $[C_{18}H_{19}Cl_2N_3O_2]$: *m/z*: 378.08; found: 378.08.

4.10.44. 3,4,5-Trimethoxy-benzoic acid (2,3,4-trihydroxy-benzylidene)-hydrazide (ME0193)

^{1}H NMR: δ 11.80 (s, 1H), 11.48 (s, 1H), 9.46 (s, 1H), 8.50 (s, 1H), 8.47 (s, 1H), 7.25 (s, 2H), 6.79 (d, J = 8.4 Hz, 1H), 6.40 (d, J = 8.4 Hz, 1H), 3.87 (s, 6H), 3.73 (s, 3H); LC–MS $[M-H^+]^-$ calcd for $[C_{17}H_{18}N_2O_7]$: *m/z*: 361.10; found: 361.14.

4.10.45. 2-Nitro-benzoic acid (2,3,4-trihydroxy-benzylidene)-hydrazide (ME0194)

Two rotamers were obtained in a 1:0.80 ratio as a result of a dynamic process. ^{1}H NMR (major rotamer): δ 12.14 (br s, 1H), 11.91 (br s, 1H), 11.08 (br s, 1H), 9.51 (br s, 1H), 8.30 (s, 1H), 8.14 (d, J = 7.3 Hz, 1H), 7.90–7.85 (m, 1H), 7.79 (d, J = 7.3 Hz, 1H), 7.77–7.73 (m, 1H), 6.83 (d, J = 8.5 Hz, 1H), 6.40 (d, J = 8.5 Hz, 1H); ^{1}H NMR (minor rotamer): δ 9.51 (br s, 1H), 9.15 (br s, 1H), 8.50 (br s, 1H), 8.37 (br s, 1H), 8.19 (dd, J = 8.2 Hz, J = 0.9 Hz, 1H), 8.13 (s, 1H), 7.90–7.85 (m, 1H), 7.79 (d, J = 7.3 Hz, 1H), 7.66 (dd, J = 7.6 Hz, J = 1.3 Hz, 1H), 6.57 (d, J = 8.6 Hz, 1H), 6.27 (d, J = 8.5 Hz, 1H); LC–MS $[M-H^+]^-$ calcd for $[C_{14}H_{11}N_3O_6]$: *m/z*: 316.05; found: 316.12.

4.10.46. 3-(4-Hydroxy-phenyl)-propionic acid (5-bromo-2-hydroxy-3-methoxy-benzylidene)-hydrazide (ME0195)

Two rotamers were obtained in a 1:0.72 ratio as a result of a dynamic process. The phenol and amide protons were exchange broadened. ^{1}H NMR (major rotamer): δ 8.30 (s, 1H), 7.37–7.31 (m, 1H), 7.15–7.09 (m, 1H), 7.06–6.98 (m, 2H), 6.69–6.62 (m,

2H), 3.82 (s, 3H), 2.85–2.73 (m, 2H), 2.50–2.42 (m, 2H); ^{1}H NMR (minor rotamer): δ 8.22 (s, 1H), 7.37–7.31 (m, 1H), 7.15–7.09 (m, 1H), 7.06–6.98 (m, 2H), 6.69–6.62 (m, 2H), 3.83 (s, 3H), 2.85–2.73 (m, 4H); LC–MS $[M-H^+]^-$ calcd for $[C_{17}H_{17}BrN_2O_4]$: *m/z*: 391.03; found: 391.18.

4.10.47. (4-Nitro-phenoxy)-acetic acid (2-hydroxy-3,5-dimethoxy-benzylidene)-hydrazide (ME0196)

Two rotamers were obtained in a 1:0.72 ratio as a result of a dynamic process. ^{1}H NMR (major rotamer): δ 11.65 (br s, 1H), 8.87 (s, 1H), 8.34 (s, 1H), 8.20 (d, J = 9.3 Hz, 2H), 7.15 (d, J = 9.3 Hz, 2H), 6.84 (d, J = 2.8 Hz, 1H), 6.63 (d, J = 2.8 Hz, 1H), 5.35 (s, 2H), 3.81 (s, 3H), 3.72 (s, 3H); ^{1}H NMR (minor rotamer): δ 11.75 (br s, 1H), 9.91 (s, 1H), 8.55 (s, 1H), 8.25 (d, J = 9.3 Hz, 2H), 7.21 (d, J = 9.3 Hz, 2H), 6.70 (d, J = 2.7 Hz, 1H), 6.65 (d, J = 2.8 Hz, 1H), 4.87 (s, 2H), 3.79 (s, 3H), 3.72 (s, 3H); LC–MS $[M-H^+]^-$ calcd for $[C_{17}H_{17}N_3O_7]$: *m/z*: 374.10; found: 374.18.

4.10.48. 2-[*N*′-(5-Bromo-2-hydroxy-3-methoxy-benzylidene)-hydrazino]-2-oxo-acetamide (ME0197)

Two rotamers were obtained in a 1:0.04 ratio as a result of a dynamic process. ^{1}H NMR (major rotamer): δ 12.47 (1H), 10.59 (br s, 1H), 8.73 (s, 1H), 8.29 (s, 1H), 7.96 (s, 1H), 7.34 (d, J = 2.1 Hz, 1H), 7.17 (d, J = 2.1 Hz, 1H), 3.83 (s, 3H); ^{1}H NMR (minor rotamer): δ 11.87 (br s, 1H), 9.85 (br s, 1H), 8.73 (s, 1H), 8.25 (s, 1H), 8.04 (s, 1H), 7.27 (d, J = 2.2 Hz, 1H), 7.13 (d, J = 2.3 Hz, 1H), 3.83 (s, 3H); LC–MS $[M-H^+]^-$ calcd for $[C_{10}H_{10}BrN_3O_4]$: *m/z*: 313.98; found: 314.04.

4.10.49. 3-Methoxy-benzoic acid (2-hydroxy-3,5-dimethoxy-benzylidene)-hydrazide (ME0198)

^{1}H NMR: δ 11.99 (br s, 1H), 10.43 (br s, 1H), 8.64 (s, 1H), 7.54–7.40 (m, 3H), 7.15 (d, J = 8.2 Hz, 1H), 6.69 (d, J = 2.6 Hz, 1H), 6.64 (d, J = 2.6 Hz, 1H), 3.83 (s, 3H), 3.80 (s, 3H), 3.74 (s, 3H); LC–MS $[M-H^+]^-$ calcd for $[C_{17}H_{18}N_2O_5]$: *m/z*: 329.11; found: 329.23.

4.10.50. 3-Chloro-benzo[*b*]thiophene-2-carboxylic acid (5-bromo-2-hydroxy-3-methoxy-benzylidene)-hydrazide (ME0199)

Two rotamers were obtained in a 1:0.31 ratio as a result of a dynamic process. The amide and phenol protons were exchange broadened. ^{1}H NMR (major rotamer): δ 8.58 (s, 1H), 8.16–8.08 (m, 1H), 8.00–7.88 (m, 1H), 7.66–7.55 (m, 2H), 7.36 (br s, 1H), 7.15–7.10 (m, 1H), 3.84 (s, 3H); ^{1}H NMR (minor rotamer): δ 8.41 (s, 1H), 8.16–8.08 (m, 1H), 8.00–7.88 (m, 1H), 7.66–7.55 (m, 2H), 7.36 (br s, 1H), 7.15–7.10 (m, 1H), 3.84 (s, 3H); LC–MS $[M-H^+]^-$ calcd for $[C_{17}H_{12}BrClN_2O_3S]$: *m/z*: 436.93; found: 437.00.

4.10.51. Isonicotinic acid (4-chloro-2-hydroxy-benzylidene)-hydrazide (ME0257)

Two rotamers were obtained in a 1:0.09 ratio as a result of a dynamic process. ^{1}H NMR (major rotamer): δ 12.27 (s, 1H), 11.37 (s, 1H), 8.84–8.76 (m, 2H), 8.67 (s, 1H), 7.88–7.79 (m, 2H), 7.67 (d, J = 8.1 Hz, 1H), 7.04–6.95 (m, 2H); ^{1}H NMR (minor rotamer): δ 12.03 (s, 1H), 10.47 (s, 1H), 8.75–8.69 (m, 2H), 8.33 (s, 1H), 7.65–7.59 (m, 2H), 7.43–7.37 (m, 1H), 6.92–6.84 (m, 2H); LC–MS $[M-H^+]^-$ calcd for $[C_{13}H_{10}ClN_3O_2]$: *m/z*: 274.04; found: 274.18.

4.10.52. Phenyl-acetic acid (5-*tert*-butyl-2-hydroxy-benzylidene)-hydrazide (ME0258)

Two rotamers were obtained in a 1:0.62 ratio as a result of a dynamic process. The phenol and amide protons were exchange broadened. ^{1}H NMR (major rotamer): δ 8.41 (s, 1H), 7.48 (d, J = 2.5 Hz, 1H), 7.37–7.19 (m, 6H), 6.86–6.79 (m, 1H), 3.56 (s, 2H), 1.25 (s, 9H); ^{1}H NMR (minor rotamer): δ 8.25 (s, 1H), 7.66 (d, J = 2.5 Hz, 1H), 7.37–7.19 (m, 6H), 6.86–6.79 (m, 1H), 3.93 (s, 2H), 1.27 (s, 9H); LC–MS $[M-H^+]^-$ calcd for $[C_{19}H_{22}N_2O_2]$: *m/z*: 309.16; found: 309.30.

4.10.53. 2-Chloro-benzoic acid (5-bromo-2-hydroxy-benzylidene)-hydrazide (ME0259)

Two rotamers were obtained in a 1:0.49 ratio as a result of a dynamic process. The phenol and amide protons were exchange broadened. ^{1}H NMR (major rotamer): δ 8.46 (s, 1H), 7.81 (d, J = 2.6 Hz, 1H), 7.63–7.41 (m, 5H), 6.90 (d, J = 8.7 Hz, 1H); ^{1}H NMR (minor rotamer): δ 8.25 (s, 1H), 7.63–7.41 (m, 4H), 7.36–7.30 (m, 2H), 6.77 (d, J = 8.6 Hz, 1H); LC–MS $[M-H^+]^-$ calcd for $[C_{14}H_{10}BrClN_2O_2]$: *m/z*: 350.95; found: 351.09.

4.10.54. 3-Methoxy-benzoic acid (5-bromo-2-hydroxy-benzylidene)-hydrazide (ME0260)

^{1}H NMR: δ 12.13 (s, 1H), 11.28 (s, 1H), 8.62 (s, 1H), 7.79 (d, J = 2.5 Hz, 1H), 7.52 (d, J = 7.8 Hz, 1H), 7.49–7.41 (m, 3H), 7.21–7.16 (m, 1H), 6.91 (d, J = 8.8 Hz, 1H), 3.84 (s, 3H); LC–MS $[M-H^+]^-$ calcd for $[C_{15}H_{13}BrN_2O_3]$: *m/z*: 347.00; found: 347.06.

4.10.55. Phenyl-acetic acid (5-bromo-2-hydroxy-benzylidene)-hydrazide (ME0261)

Two rotamers were obtained in a 1:0.72 ratio as a result of a dynamic process. The phenol and amide protons were exchange broadened. ^{1}H NMR (major rotamer): δ 8.37 (s, 1H), 7.74 (d, J = 2.6 Hz, 1H), 7.43–7.19 (m, 6H), 6.89–6.83 (m, 1H), 3.56 (s, 2H); ^{1}H NMR (minor rotamer): δ 8.21 (s, 1H), 7.80 (d, J = 2.6 Hz, 1H), 7.43–7.19 (m, 6H), 6.89–6.83 (m, 1H), 3.96 (s, 2H); LC–MS $[M-H^+]^-$ calcd for $[C_{15}H_{13}BrN_2O_2]$: *m/z*: 331.01; found: 331.18.

4.10.56. Phenyl-acetic acid (5-bromo-2-hydroxy-3-methoxy-benzylidene)-hydrazide (ME0262)

Two rotamers were obtained in a 1:0.78 ratio as a result of a dynamic process. ^{1}H NMR (major rotamer): δ 11.87 (s, 1H), 10.76 (s, 1H), 8.38 (s, 1H), 7.34 (d, J = 2.3 Hz, 1H), 7.34–7.19 (m, 5H), 7.14 (d, J = 2.3 Hz, 1H), 3.82 (s, 3H), 3.55 (s, 2H); ^{1}H NMR (minor rotamer): δ 11.41 (s, 1H), 9.63 (s, 1H), 8.25 (s, 1H), 7.43 (d, J = 2.4 Hz, 1H), 7.34–7.19 (m, 5H), 7.12 (d, J = 2.3 Hz, 1H), 3.95 (s, 2H), 3.84 (s, 3H); LC–MS $[M-H^+]^-$ calcd for $[C_{16}H_{15}BrN_2O_3]$: *m/z*: 361.02; found: 361.06.

4.10.57. 4-Methyl-benzoic acid (5-*tert*-butyl-2-hydroxy-benzylidene)-hydrazide (ME0263)

^{1}H NMR: δ 12.01 (s, 1H), 11.12 (s, 1H), 8.63 (s, 1H), 7.85 (d, J = 8.2 Hz, 2H), 7.49 (d, J = 2.5 Hz, 1H), 7.39–7.31 (m, 3H), 6.87 (d, J = 8.6 Hz, 1H), 2.39 (s, 3H), 1.28 (s, 9H); LC–MS $[M-H^+]^-$ calcd for $[C_{19}H_{22}N_2O_2]$: *m/z*: 309.16; found: 309.30.

4.10.58. 4-Nitro-benzoic acid (3-fluoro-2-hydroxy-benzylidene)-hydrazide (ME0264)

Two rotamers were obtained in a 1:0.09 ratio as a result of a dynamic process. For the minor rotamer, the phenol and amide protons were exchange broadened. ^{1}H NMR (major rotamer): δ 12.48 (s, 1H), 11.44 (s, 1H), 8.70 (s, 1H), 8.43–8.37 (m, 2H), 8.22–8.15 (m, 2H), 7.44 (d, J = 7.8 Hz, 1H), 7.34–7.26 (m, 1H), 6.97–6.89 (m, 1H); ^{1}H NMR (minor rotamer): δ 8.43–8.30 (m, 3H), 8.01–7.94 (m, 2H), 7.26–7.16 (m, 2H), 6.82 (br s, 1H); LC–MS $[M-H^+]^-$ calcd for $[C_{14}H_{10}FN_3O_4]$: *m/z*: 302.06; found: 302.15.

Acknowledgements

We thank the Swedish National Research Council, the Swedish Governmental Agency for Innovation Systems (VINNOVA), the Carl Trygger foundation, and Creative Antibiotics for support. The work was carried out with affiliation to Umeå Centre for Microbial Research.

Supplementary data

Supplementary data associated with this article can be found, in the online version, at doi:10.1016/j.bmc.2010.02.022.

References and notes

1. Marra, A. *Drugs R. D.* **2006**, 7.
2. Clatworthy, A. E.; Pierson, E.; Hung, D. T. *Nat. Chem. Biol.* **2007**, *3*, 541.
3. Escaich, S. *Curr. Opin. Chem. Biol.* **2008**, *12*, 400.
4. Hueck, C. J. *Microbiol. Mol. Biol. Rev.* **1998**, *62*, 379.
5. Keyser, P.; Elofsson, M.; Rosell, S.; Wolf-Watz, H. *J. Int. Med.* **2008**, *264*, 17.
6. Kauppi, A. M.; Nordfelth, R.; Uvell, H.; Wolf-Watz, H.; Elofsson, M. *Chem. Biol.* **2003**, *10*, 241.
7. Gauthier, A.; Robertson, M. L.; Lowden, M.; Ibarra, J. A.; Puente, J. L.; Finlay, B. B. *Antimicrob. Agents Chemother.* **2005**, *49*, 4101.
8. Linington, R. G.; Robertson, M.; Gauthier, A.; Finlay, B. B.; MacMillan, J. B.; Molinski, T. F.; van Soest, R.; Andersen, R. J. *J. Nat. Prod.* **2006**, *69*, 173.
9. Felise, H. B.; Nguyen, H. V.; Pfuetzner, R. A.; Barry, K. C.; Jackson, S. R.; Blanc, M. P.; Bronstein, P. A.; Kline, T.; Miller, S. I. *Cell Host Microbe* **2008**, *4*, 325.
10. Iwatsuki, M.; Uchida, R.; Yoshijima, H.; Ui, H.; Shiomi, K.; Matsumoto, A.; Takahashi, Y.; Abe, A.; Tomoda, H.; Omura, S. *J. Antibiot.* **2008**, *61*, 222.
11. Pan, N. J.; Brady, M. J.; Leong, J. M.; Goguen, J. D. *Antimicrob. Agents Chemother.* **2009**, *53*, 385.
12. Kauppi, A. M.; Nordfelth, R.; Hagglund, U.; Wolf-Watz, H.; Elofsson, M. *Adv. Exp. Med. Biol.* **2003**, *529*, 97.
13. Nordfelth, R.; Kauppi, A. M.; Norberg, H. A.; Wolf-Watz, H.; Elofsson, M. *Infect. Immun.* **2005**, *73*, 3104.
14. Sun, J. S.; Han, X. W.; Yu, B. *Synlett* **2005**, 437.
15. Tsuchiya, S.; Sunazuka, T.; Hirose, T.; Mori, R.; Tanaka, T.; Iwatsuki, M.; ÅŒmura, S. *Org. Lett.* **2006**, *5577*, 8.
16. Kauppi, A. M.; Andersson, C. D.; Norberg, H. A.; Sundin, C.; Linusson, A.; Elofsson, M. *Bioorg. Med. Chem.* **2007**, *15*, 6994.
17. Dahlgren, M. K.; Kauppi, A. M.; Olsson, I.-M.; Linusson, A.; Elofsson, M. *J. Med. Chem.* **2007**, *50*, 6177.
18. Kline, T.; Felise, H. B.; Barry, K. C.; Jackson, S. R.; Nguyen, H. V.; Miller, S. I. *J. Med. Chem.* **2008**, *51*, 7065.
19. Kline, T.; Barry, K. C.; Jackson, S. R.; Felise, H. B.; Nguyen, H. V.; Miller, S. I. *Bioorg. Med. Chem. Lett.* **2009**, *19*, 1340.
20. Yang, S.; Peng, Q.; San Francisco, M.; Wang, Y.; Zeng, Q.; Yang, C.-H. *PLoS ONE* **2008**, *3*, e2973.
21. Li, Y.; Peng, Q.; Selimi, D.; Wang, Q.; Charkowski, A. O.; Chen, X.; Yang, C. H. *Appl. Environ. Microb.* **2009**, *75*, 1223.
22. Puiac, S.; Negrea, A.; Richter-Dahlfors, A.; Plant, L.; Rhen, M. *Antimicrob. Agents. Chemother.* **2009**, *53*, 2402.
23. Wolf, K.; Betts, H. J.; Chellas-Gery, B.; Hower, S.; Linton, C. N.; Fields, K. A. *Mol. Microbiol.* **2006**, *61*, 1543.
24. Negrea, A.; Bjur, E.; Ygberg, S. E.; Elofsson, M.; Wolf-Watz, H.; Rhen, M. *Antimicrob. Agents Chemother.* **2007**, *51*, 2867.
25. Hudson, D. L.; Layton, A. N.; Field, T. R.; Bowen, A. J.; Wolf-Watz, H.; Elofsson, M.; Stevens, M. P.; Galyov, E. E. *Antimicrob. Agents. Chemother.* **2007**, *51*, 2631.
26. Veenendaal, A. K. J.; Sundin, C.; Blocker, A. J. *J. Bacteriol.* **2009**, *191*, 563.
27. Tree, J. J.; Wang, D.; McInally, C.; Mahajan, A.; Layton, A.; Houghton, I.; Elofsson, M.; Stevens, M. P.; Gally, D. L.; Roe, A. J. *Infect. Immun.* **2009**, *77*, 4209.
28. Muschiol, S.; Bailey, L.; Gylfe, A.; Sundin, C.; Hultenby, K.; Bergstrom, S.; Elofsson, M.; Wolf-Watz, H.; Normark, S.; Henriques-Normark, B. A. *Proc. Natl. Acad. Sci. U.S.A.* **2006**, *103*, 14566.
29. Bailey, L.; Gylfe, A.; Sundin, C.; Muschiol, S.; Elofsson, M.; Nordstrom, P.; Henriques-Normark, B.; Lugert, R.; Waldenstrom, A.; Wolf-Watz, H.; Bergstrom, S. *FEBS Lett.* **2007**, *581*, 587.
30. Slepenkin, A.; Enquist, P. A.; Hagglund, U.; de la Maza, L. M.; Elofsson, M.; Peterson, E. M. *Infect. Immun.* **2007**, *75*, 3478.
31. Muschiol, S.; Normark, S.; Henriques-Normark, B.; Subtil, A. *BMC Microbiol.* **2009**, *9*, 75.
32. Prantner, D.; Nagarajan, U. M. *Infect. Immun.* **2009**, *77*, 76.
33. Hansch, C. A. *Acc. Chem. Res.* **1969**, *2*, 232.
34. Wold, S.; Dunn, W. J., III *J. Chem. Inf. Model.* **1983**, *23*, 6.
35. Eriksson, L.; Johansson, E. *Chemom. Intell. Lab. Syst.* **1996**, *34*, 1.
36. Martin, E. J.; Blaney, J. M.; Siani, M. A.; Spellmeyer, D. C.; Wong, A. K.; Moos, W. H. *J. Med. Chem.* **1995**, *1431*, 38.
37. Linusson, A.; Wold, S.; Norden, B. *Mol. Divers.* **1999**, *4*, 103.
38. Holm, L.; Frech, K.; Dzhambazov, B.; Holmdahl, R.; Kihlberg, J.; Linusson, A. *J. Med. Chem.* **2007**, *50*, 2049.
39. Larsson, A.; Johansson, S.; Pinkner, J. S.; Hultgren, S. J.; Almqvist, F.; Kihlberg, J.; Linusson, A. *J. Med. Chem.* **2005**, *48*, 935.
40. Linusson, A.; Gottfries, J.; Olsson, T.; Örnskov, E.; Folestad, S.; Norden, B.; Wold, S. *J. Med. Chem.* **2001**, *44*, 3424.
41. Nurbo, J.; Roos, A. K.; Muthas, D.; Wahlstrom, E.; Ericsson, D. J.; Lundstedt, T.; Unge, T.; Karlen, A. *J. Pept. Sci.* **2007**, *13*, 822.
42. Davies, M. *J. Am. Stat. Assoc.* **1961**, *56*, 729.
43. Wold, S. R. A.; Wold, H.; Dunn, W. I. *SIAM J. Sci. Stat. Comp.* **1984**, *5*, 735.
44. Wold, S.; Sjostrom, M.; Eriksson, L. *Chemom. Intell. Lab. Syst.* **2001**, 58.
45. Cortes, C.; Vapnik, V. *Mach. Learn.* **1995**, *20*, 273.
46. Matthews, E. J.; Kruhlak, N. L.; Benz, R. D.; Contrera, J. F.; Marchant, C. A.; Yang, C. *Toxicol. Mech. Methods* **2008**, *18*, 189.
47. Zhu, H.; Tropsha, A.; Fourches, D.; Varnek, A.; Papa, E.; Gramatica, P.; Oberg, T.; Dao, P.; Cherkasov, A.; Tetko, I. V. *J. Chem. Inf. Model.* **2008**, *48*, 766.
48. Muchmore, S. W.; Debe, D. A.; Metz, J. T.; Brown, S. P.; Martin, Y. C.; Hajduk, P. J. *J. Chem. Inf. Model.* **2008**, *48*, 941.
49. Olsson, I. M.; Gottfries, J.; Wold, S. *Chemom. Intell. Lab. Syst.* **2004**, *73*, 37.
50. Tauschek, M.; Gorrell, R. J.; Strugnell, R. A.; Robins-Browne, R. M. *Proc. Natl. Acad. Sci. U.S.A.* **2002**, *99*, 7066.
51. Kaper, J. B.; Nataro, J. P.; Mobley, H. L. T. *Nat. Rev. Microbiol.* **2004**, *2*, 123.
52. Cornelis, G. R. *Nat. Rev. Microbiol.* **2006**, *4*, 811.
53. Koh, L. L.; Kon, O. L.; Loh, K. W.; Long, Y. C.; Ranford, J. D.; Tan, A. L. C.; Tjan, Y. Y. *J. Inorg. Biochem.* **1998**, *72*, 155.
54. Gudasi, K.; Patil, M.; Vadavi, R.; Shenoy, R.; Patil, S.; Nethaji, M. *Transition Met. Chem.* **2006**, *31*, 580.
55. Zu, D.; Liu, R. C. H. *Med. Res. Rev.* **2002**, *22*, 26.
56. MOE. *Molecular Operating Environment (MOE), Version 2005.06*, Chemical Computing Group, Inc.: Montreal, Quebec, Canada, 2005.
57. OMEGA. *OpenEye Scientific Software, Inc.*, 2.3.2; 9 Bisbee, Suite D, Santa FE, New Mexico, United States of America.
58. Jaguar. *Version 6.5*, Schrödinger, LLC, New York, NY, 2006.
59. Umetrics. *SIMCA-P+* 12.0; Box 7960, S-907 19 Umeå, Sweden.
60. MODDE. *Umetrics*, 8; Box 7960, S-907 19 Umeå, Sweden.
61. Lindgren, F.; Hansen, B.; Karcher, W.; Sjostrom, M.; Eriksson, L. *J. Chemom.* **1996**, *10*, 521.
62. Wold, S. *Pattern Recognit.* **1976**, *8*, 127.
63. O'Brien, J.; Wilson, I.; Orton, T.; Pognan, F. *Eur. J. Biochem.* **2000**, *267*, 5421.
64. Lindhagen-Persson, M.; Vestling, M.; Reixach, N.; Olofsson, A. *Amyloid* **2008**, *15*, 240.